ISTANBUL TECHNICAL UNIVERSITY ★ GRADUATE SCHOOL

ANTHROPOMETRIC MEASUREMENTS FROM IMAGES

M.Sc. THESIS

Rumeysa Aslıhan ERTÜRK

Department of Computer Engineering

Computer Engineering Programme

JULY 2023

ISTANBUL TECHNICAL UNIVERSITY ★ GRADUATE SCHOOL

ANTHROPOMETRIC MEASUREMENTS FROM IMAGES

M.Sc. THESIS

Rumeysa Aslıhan ERTÜRK
(504201535)

Department of Computer Engineering

Computer Engineering Programme

Thesis Advisor: Prof. Dr. Mustafa Ersel KAMAŞAK
Co-advisor: Prof. Dr. Oğuzhan KÜLEKCİ

JULY 2023

İSTANBUL TEKNİK ÜNİVERSİTESİ ★ LİSANSÜSTÜ EĞİTİM ENSTİTÜSÜ

FOTOĞRAFLARDAN ANTROPOMETRİK ÖLÇÜMLER

YÜKSEK LİSANS TEZİ

Rumeysa Aslıhan ERTÜRK
(504201535)

Bilgisayar Mühendisliği Anabilim Dalı

Bilgisayar Mühendisliği Programı

Tez Danışmanı: Prof. Dr. Mustafa Ersel KAMAŞAK
Eş Danışman: Prof. Dr. Oğuzhan KÜLEKCİ

TEMMUZ 2023

Rumeysa Aslıhan ERTÜRK, a M.Sc. student of ITU Graduate School student ID 504201535 successfully defended the thesis entitled "ANTHROPOMETRIC MEASUREMENTS FROM IMAGES", which he/she prepared after fulfilling the requirements specified in the associated legislations, before the jury whose signatures are below.

Thesis Advisor :	**Prof. Dr. Mustafa Ersel KAMAŞAK** Istanbul Technical University	....
Co-advisor :	**Prof. Dr. Oğuzhan KÜLEKCİ** Istanbul Technical University	....
Jury Members :	**Prof. Dr. Behçet Uğur TÖREYİN** Istanbul Technical University	....
	Assoc. Prof. Dr. Gökhan BİLGİN Yıldız Technical University	....
	Asst. Prof. Dr. Metin ERTAŞ Istanbul University	....

Date of Submission : **26 May 2023**
Date of Defense : **18 July 2023**

To my dearest family,

FOREWORD

I thank my thesis advisor Prof. Dr. Mustafa Ersel Kamaşak for his support throughout this journey.

My time at Istanbul Technical University has improved me a lot, not just academically but also socially and intellectually. I cannot underestimate the support I received from my professors, colleagues, friends, and my students. Their motivational support and constructive criticisms made this project a reality.

I sincerely thank the subjects who voluntarily participated in the experiments I conducted in the scope of this project. Without them, this project would not have been completed.

I thank, from the deepest part of my heart, my family: my lovely mother, Gönül ERTÜRK, who has always been there for me; my dearest father, Alim ERTÜRK, whose support I always feel behind me; my gorgeous siblings Nursena and Muhammet Emin, who are the source of my joy. I would not be here if it were not for all of you.

July 2023 Rumeysa Aslıhan ERTÜRK

TABLE OF CONTENTS

ABBREVIATIONS

OS	: Operating System
PC	: Personal Computer
WHR	: Waist-to-Hip Ratio
WHtR	: Waist-to-Height Ratio
BMI	: Body Mass Index
WC	: Waist Circumference
BC	: Bust Circumference
HC	: Hip Circumference
CNN	: Convolutional Neural Network
ML	: Machine Learning
k-NN	: k-Nearest Neighbors
SVR	: Support Vector Regression
DTR	: Decision Tree Regression
TF	: TensorFlow
MP	: Megapixels
CDC	: Center for Disease Control and Prevention
2D	: 2-Dimensional
3D	: 3-Dimensional

SYMBOLS

V	:	Volts
$\mathbf{c_t}$	:	Transformation Constant
$\mathbf{d_k}$	:	Known Distance
$\mathbf{d_l}$	:	Distance Between Lasers
a	:	Major Axis of the Ellipse
b	:	Minor Axis of the Ellipse
C	:	Circumference of the Ellipse
$\mathbf{m_M}$	:	Manual Measurement
$\mathbf{m_A}$	:	Automatic Measurement
$\mathbf{E_r}$	:	Relative Error

LIST OF TABLES

Page

LIST OF FIGURES

ANTHROPOMETRIC MEASUREMENTS FROM IMAGES

SUMMARY

In this work, a system that simultaneously estimates several anthropometric measurements (namely, height and the circumferences of the bust, waist, and hip) using only two 2D images of a human subject has been proposed and tested.

The proposed system has two components: a customized camera setup with four laser pointers and image analysis software. The camera setup includes an Android smartphone, four laser pointers around the smartphone's camera, and a tripod carrying the hardware. The image analysis software is a web-based application that has not been publicly available. The application takes the images as input, processes them, and yields the aforementioned anthropometric measurements in the unit of centimeters.

The pipeline of the proposed system has the following components:

1. Feeding the images to the software,
2. Determining the locations of the body parts that will be measured,
3. Calculating the width of the body part on the specific location in both images (anterior and lateral),
4. Transforming pixel widths into physical units,
5. Estimating the circumference of the body part (or the height).

For determining the locations of the body parts that will be measured, the software model applies pre-trained pose estimation and body segmentation models to both input images. For pose estimation, the MediaPipe framework, a tool developed for constructing pipelines based on sensory data, has been used. For body segmentation, BodyPix 2.0 in TensorFlow, a powerful tool that can perform whole-body segmentation on humans in real time, has been adopted. With the help of these models, body parts to be measured has been located on the input images.

The width of a body part is measured as the largest distance between the left and right sides of the specific body part on the image. Laser points attached to the camera are leveraged while transforming pixel widths into physical units (i.e., centimeters).

The last step of the measurements is converting the width into circumference. It is assumed that the cross-sectional areas of the body parts that are focused on in this research, namely, the bust, waist, and hip, are elliptical, and the circumferences of these body parts correspond to the perimeters of these ellipses. With the axes of the ellipses in hand, it is possible to estimate these anthropometric measurements.

In order to evaluate the performance of the model, experiments were done on 19 volunteer human subjects. The actual measurements of these subjects were collected

with traditional manual methods. The results obtained from the proposed model were compared with the actual measurements of the subjects, and the relative percentage errors were evaluated.

The proposed hardware is a developed version of the prototype that was designed to assess the validity of the idea. The experiments described in this work, include the previous version of the proposed camera setup for better analysis and comparison. During the image collection stage of the experiment, the subjects that participated in the experiments are photographed with both versions of the camera setup, and the images are processed with software that is calibrated for individual camera setups.

Finally, collected images are fed to a commercially available system that creates 3D meshes of humans from 2D images. This product can estimate body measurements from these meshes. For comparing the proposed system to a commercial product, this tool is included to the experiments.

The images collected from the subjects who participated in the experiment are processed with the three systems mentioned earlier: the initial prototype, the improved version, and the commercially available tool. The results show that the initial prototype's relative errors for the bust, waist, and hip circumferences and height are 7.32%, 9.7%, 7.12%, and 5.0%, respectively. For the improved version, the errors become 15.97%, 9.92%, 2.01%, and 4.43%. The commercial product included in the study has relative errors of 7.8%, 10.69%, 12.43%, and 3.33% for the aforementioned body measurements.

The main advantage of the proposed system over the alternative automatic methods is that, unlike the state-of-the-art measuring techniques, our method does not require predefined environmental conditions such as a specific background, a predetermined distance from the camera, or some clothing constraints. The lack of these restrictions makes the proposed system adaptable to various conditions, such as indoor and outdoor environments. The target user profile for this application would be medical practitioners, personal trainers, and individuals who want to keep track of their weight-loss progress since the system is lightweight, easy to use, and adaptable to various environments.

FOTOĞRAFLARDAN ANTROPOMETRİK ÖLÇÜMLER

ÖZET

Bu çalışmada, bir insan deneğin sadece iki 2 boyutlu görüntüsünü kullanarak birkaç antropometrik ölçümü (boy, göğüs, bel ve kalça çevreleri) aynı anda yapan bir sistem önerilmiş ve test edilmiştir.

Önerilen sistemin iki bileşeni bulunmaktadır: dört lazer işaretleyicili özelleştirilmiş bir kamera ekipmanı ve bir görüntü analiz yazılımı. Kamera düzeneği bir Android akıllı telefon, akıllı telefonun kamerasının etrafına yerleştirilmiş dört lazer işaretçi ve donanımı taşıyan bir tripod içermektedir. Görüntü analiz yazılımı, henüz kamunun kullanımına sunulmamış web tabanlı bir uygulaya entegre halde tasarlanmıştır. Uygulama, görüntüleri girdi olarak almakta, işlemekte ve yukarıda bahsedilen antropometrik ölçümleri santimetre cinsinden vermektedir.

Önerilen sistemin boru hattı şu bileşenlere sahiptir:

1. Görüntülerin yazılıma beslenmesi,
2. Ölçülecek vücut parçalarının konumlarının belirlenmesi,
3. Her iki görüntüde de (ön ve yan) belirli konumdaki vücut parçasının genişliğinin hesaplanması,
4. Piksel genişliklerinin fiziksel birimlere dönüştürülmesi,
5. Vücut parçasının çevresinin tahmin edilmesi.

Ölçülecek vücut parçalarının konumlarını belirlemek için yazılım modeli, girdi olarak kullanılan her iki görüntüye de önceden eğitilmiş poz tahmini ve vücut segmentasyon modellerini uygular. Poz tahmini görevi için, duyusal verilere dayalı boru hatları oluşturmak amacıyla geliştirilmiş bir çerçeve olan MediaPipe aracı kullanılmıştır. Vücut segmentasyonu için TensorFlow kütüphanesinde bulunan, insanlar üzerinde gerçek zamanlı olarak tam vücut segmentasyonu gerçekleştirebilen çok güçlü bir araç olan BodyPix 2.0 kullanılmıştır. Bu modeller yardımıyla, çevresi ölçülecek vücut parçalarının konumları başarıyla belirlenebilmiştir.

Bir vücut parçasının genişliği, görüntü üzerinde ilgili vücut parçasının sol ve sağ sınırları arasındaki en büyük mesafe olarak ölçülmüştür. Örneğin, kalça bölgesi için piksel cinsinden genişlik, vücut segmentasyon işlemi ile bulunmuş ilgili bölgenin yataydaki genişliğidir.

Piksel genişlikleri fiziksel birimlere (örneğin santimetre) dönüştürülürken kameraya bağlı lazer noktalarından yararlanılır. Bu yöntemin doğru çalışabilmesi için kameranın etrafındaki lazer noktaları arasındaki mesafenin sabit olması gerekmektedir. Bu mesafe, donanım geliştirilirken belirlenmiş ve buna göre üretilmiştir. Deneklerin

fotoğraflarında üzerlerine düşmüş olan lazer noktaları arasındaki mesafe, deneğin kameraya uzaklığına göre değişeceğinden bu uzaklık, her deneğin her görseli için tekrar ölçülmelidir. Görsel üzerinden ölçülmüş bu mesafe piksel cinsinden olacaktır. Bu değerin standart birimdeki karşılığı, kameranın üzerindeki lazerlerin standart birim cinsinden uzaklığı olduğundan normalizasyon işlemi bu bilgi kullanılarak yapılabilir. Başka bir deyişle, kameranın etrafına entegre edilmiş olan lazer noktaları, görselde iki piksel arasındaki uzaklığın gerçek dünyadaki karşılığını bulmak için kullanılmaktadır. Bu dönüşüm kullanılarak vücut bölgelerinin genişliği standart birime aktarılabilmektedir.

Ölçümlerin son adımı fotoğraflardan alınan genişlik ölçülerinin vücut parçalarının çevrelerine dönüştürülmesidir. Bu çalışma kapsamında ilgilenilen vücut parçalarının (yani göğüs, bel ve kalça) kesit alanlarının elips şeklinde olduğu ve bu vücut parçalarının çevrelerinin bu elipslerin çevrelerine karşılık geldiğini varsayılmıştır. Bir elipsin çevresinin bulunması için kendisine ait majör ve minör eksenlerin uzunluklarının bilinmesi gerekir. Yukarıda anlatılan yönteme göre deneğin önden (anterior) çekilmiş fotoğrafında, ilgili vücut parçasına ait genişlik, elipsin majör eksenine denk gelirken, deneğin yan tarafından (lateral) alınmış görüntüdeki genişlik elipsin minör eksenine tekabül etmektedir. Böylece, majör ve minör eksen uzunlukları tespit edilmiş elipsin çevresi cebirsel formüllerle hesaplanabilmektedir.

Çalışma kapsamında son vücut ölçüsü, deneklerin boy uzunluklarıdır. Deneklerin boyları, yalnızca profilden çekilmiş görüntüler kullanılarak (lateral) hesaplanmıştır. Buna göre, ilgili görüntüde vücut segmentasyon modelinin yardımıyla deneğin baş ve ayak bölgeleri tespit edilmiştir. Bu iki bölge arasındaki en büyük uzaklığın deneğin boyuna tekabül ettiği varsayımıyla ölçüm yazılımı tasarlanmıştır.

Geliştirilen modelin performansını değerlendirmek için gönüllü 19 insan denek üzerinde deneyler yapılmıştır. Bu deneklerin gerçek ölçüleri geleneksel manuel yöntemlerle toplanmıştır. Önerilen modelden elde edilen sonuçlar, deneklerin gerçek ölçümleri ile karşılaştırılarak göreceli hata yüzdeleri değerlendirilmiştir.

Bu çalışmada tanıtılan sistem, prototip olarak oluşturulmuş ilk donanım ve yazılım modelinin geliştirilmiş bir versiyonudur. Daha iyi bir performans analizi için, önerilen kamera kurulumunun önceki versiyonu da deneylere dahil edilmiştir. Deneyin görüntü toplama aşamasında, deneklerin kamera kurulumunun her iki versiyonu ile fotoğrafları çekilmiş ve bu görüntüler her bir kamera kurulumlarına göre kalibre edilmiş yazılımlarla işlenmiştir.

Son olarak, toplanan görüntüler, 2 boyutlu görüntülerden 3 boyutlu insan vücut ağları oluşturan ve piyasaya ticari bir ürün olarak sürülmüş bir sisteme girdi olarak verilmiştir. Bu ürün, insan vücudunun 3B ağ modelincen vücut ölçülerini tahmin etme özelliğine sahiptir. Bu proje kapsamında toplanan görüntüler, önerilen modelin daha ayrıntılı bir karşılaştırması için bu yazılıma beslenmiş ve çıktıları karşılaştırma amacıyla sunulmuştur.

Deney 19 insan denek (4 kadın, 15 erkek) üzerinde yürütülmüştür. Önerilen kamera sisteminin üretilen ilk versiyonuyla yapılan deneylerde göğüs, bel ve kalça çevresi ile boy uzunluğu ölçüm hataları sırasıyla %7.32, %9.7, %7.12 ve %5.0 olarak hesaplanmıştır. Geliştirilmiş ikinci versiyona bu hataların %15.9, %9.92, %2.01

ve %4.43 olduğu görülmüştür. Son olarak, kıyas amaçlı deneye dahil edilen 3 boyutlu insan modellemesi yapan sistemin ilgili vücut bölgelerdeki ortalama göreli hata oranlarısırasıyla %7.8, %10.69, %12.43 ve %3.33 olarak ölçülmüştür.

Yapılan deneylerin sonuçları dikkate alındığında, görülmüştür ki çevre koşulları sistemin çıktısı üzerinde çok önemli bir etkiye sahiptir. Görüntünün alındığı ortamın ışıklandırma sistemi, ortam ışığının gücü ve yansıma oranı gibi dış etkenlerin önerilen sistemin performansına gözle görülür oranda etki etmektedir. Benzer şekilde, deneklerin üzerindeki kıyafetlerin kalıbı ve renginin de ölçüm sonuçlarını ciddi derecede etkilediği saptanmıştır. Koyu renkli ve ışığı soğuran dokuya sahip giysiler lazer noktalarını yansıtmadığından yazılım görsel üzerinde bu noktaları saptayamamakta ve sistem vücut ölçülerini almayı başaramamaktadır. Böyle giysilerle deneye katılan deneklerin görüntüleri ölçümlere dahil edilmemişlerdir.

Bazı vücut bölgelerinin ölçümlerindeki yüksek hata oranlarının tek kaynağının önerilen donanım ya da yazılım olmayabileceği de not edilmelidir. Zira deneklerin gerçek vücut ölçülerini almak için kullanılan ölçüm yöntemi de hataya açıktır. Bu hatanın sebebi ölçüm aleti olabileceği gibi ölçen kişinin bilgisizliği veya tecrübesizliği de olabilmektedir. Bu çalışmayı yürütenlerin uzmanlık alanı tıbbi bilimler değil de mühendislik olduğundan, gerçek ölçülerin alınması sırasında hatalar olması olasıdır. Bundan kaynaklanan hataların, geliştirilen sistemin hatası gibi görünebileceği de göz önünde bulundurulmalıdır. Bir başka deyişle, elde edilen hata değerlerinin tek kaynağı önerilen modelin başarısızlığı olmayabilir.

Önerilen sistemin alternatif yöntemlere göre en büyük avantajı, en gelişmiş otomatik antropometrik ölçüm tekniklerinin aksine, belirli bir arka plan, kameradan belirli bir uzaklıkta olunması veya bazı kıyafet kısıtlamaları gibi önceden tanımlanmış çevresel koşullar gerektirmemesidir. Bu tür kısıtlamaların olmaması, önerilen sistemi iç ve dış ortamlar gibi çeşitli koşullarda kullanıma müsait hale getirmektedir. Sistem hafif, kullanımı kolay ve farklı ortamlara uyarlanabilir olduğundan, bu uygulama için hedef kullanıcı profili tıp pratisyenleri, kişisel spor eğitmenleri ve kilo verme ilerlemelerini takip etmek isteyen bireyler olacaktır.

1. INTRODUCTION

1.1 Purpose of Thesis

Anthropometric measurements refer to non-invasive quantitative measurements of the human body. These measurements include commonly used indicators such as height, weight, body mass index (BMI), and various circumferences, such as those of the waist, hip, neck, and head [1]. These measurements, along with their ratios such as waist-to-hip [2] and waist-to-height [3,4], are valuable tools for clinicians in monitoring various aspects. They help track factors like the growth and nutritional status of children and the risks of obesity, diabetes, and cardiovascular diseases in adults [5]–[12].

When obtaining anthropometric measurements, healthcare professionals typically rely on manual tools such as weight scales, calibration weights, stadiometers, knee calipers, and non-stretchable tape measures [1]. However, despite their simplicity and cost-effectiveness, these traditional manual methods suffer from several limitations. For example, they (a) consume a significant amount of time, (b) necessitate calibrated equipment and skilled practitioners, and (c) are heavily influenced by the conditions of the individual being measured and the specified measuring procedure, which diminishes the reproducibility of the obtained results [13].

Nowadays, there has been a growing trend in the research of advanced anthropometric measurements that utilize 3D scanned images of individuals [14,15]. Numerous studies have demonstrated that these automated 3D scanners provide precise and consistent measurements comparable to those obtained manually [13,16,17]. However, it is essential to note that this method necessitates specialized equipment for capturing the subject's images.

Another alternative researchers explore involves using 2D images instead of 3D, intending to simplify the measurement process. Several studies have indicated that employing 2D images also yields satisfactory results [18]–[20].

This project focuses on developing a user-friendly measuring application that eliminates complex hardware needs. It can be easily used by many individuals, including medical practitioners, personal trainers, and those monitoring their weight-loss progress. For this purpose, a system that contains hardware and software components has been created and tested. The system utilizes two 2D images (one from the anterior view and one from the lateral view) of a human subject, captured using a lightweight laser pointer system and a mobile phone. The application then provides measurements for height and circumferences of the bust, waist, and hip regions.

1.2 Literature Review

Throughout history, the measurement of the human body has served various purposes. In ancient times, body measurement was primarily employed in the realm of figurative arts. Over time, this practice extended its utility to the fields of naturalism and anthropology, allowing for the identification of fundamental morphological characteristics in humans [21].

Anthropometric measurements involve noninvasive quantitative assessments of the body. These measurements play a crucial role in evaluating nutritional status, general health, and growth patterns in both children and adults, as stated by the Centers for Disease Control and Prevention (CDC). In the pediatric population, these measurements are precious for assessing overall health and nutritional adequacy besides monitoring the growth and development of children. They serve as reliable indicators of a child's health and well-being. Body measurements are helpful for adults in evaluating health, dietary status, and predicting the risk of future diseases. Additionally, these measurements can be utilized to assess body composition, aiding in determining nutritional status and the diagnosis of obesity [8].

Medical practitioners widely use anthropometric measurements since they can be indicators of various kinds of diseases. For years, relationships between diseases and anthropometric measurements have been detected with the help of statistical studies. According to the studies, waist circumference (WC) can be an indicator of type-2 diabetes [22], obesity [23], high blood pressure [24], impaired glucose tolerance [25], and cardiovascular diseases [10,26]. Similarly, hip circumference (HC) is found to be a good metric for type-2 diabetes [11,27], cardiovascular and [28] coronary heart diseases [27,29]. In addition to circumferences of specific body regions, their ratios with respect to each other are also great metrics that can be used for diagnoses or risk evaluations. Some studies suggest that waist-to-height ratio (WHtR) is a good indicator for conditions such as lipidemia [30], type-2 diabetes [31], impaired fasting glucose [31], cardiometabolic [32], and cardiovascular [33] diseases, and obstructive sleep apnea syndrome [34]. Researches conducted on the waist-to-hip ratio (WHR) show that this value is a good metric for conditions such as all-cause mortality [35], obesity [36], cardiovascular diseases [37] and hypertension [38]. Therefore, undoubtedly, collecting anthropometric measurements fast and accurately holds significant importance in medical studies.

Traditionally, for taking anthropometric measurements, manual tools such as weight scales, calibration weights, stadiometers, knee calipers, and non-stretchable tape measures [1] is used by healthcare professionals. Nevertheless, these conventional manual techniques have various drawbacks despite being simple and cost-effective. For instance, they (a) require a substantial time investment, (b) rely on calibrated equipment and proficient operators, and (c) are greatly affected by the individual's conditions and the specific measurement process, thereby reducing the reproducibility of the results obtained [13]. Hence, with the developing technology, obtaining anthropometric measurements with the help of digital tools is getting more popular.

Previous studies on this topic can be grouped into two categories: the ones that use 2D images [19,39]–[43] for measurements, and the ones where 3D scanning [44]–[47] techniques are employed.

The proposed system has been inspired by several studies in the literature. One of them, conducted in 2004, shares a common intention and estimates several anthropometric measurements from 2D images taken from different angles. In their research, Hung et al. [19] developed and tested a system in which they take photographs of human subjects from 3 positions, specifically front, side, and back, intending to measure 10 different body measurements from the images digitally. Their system is human-assisted, and the testers involved in the study pin important landmarks of the image, and the measurements are calculated using those landmarks. For some body parts, they assume an elliptical cross-sectional area; for others, they assume a shape that combines a rectangle and an ellipse. They use a black square seen in the images, whose dimensions in the real world are known, so they can use it as a reference while transforming from pixel to metric space. They assess the performance of their proposed system by comparing the real measurements of the human subjects taken manually with the automatic estimations done by their system. They use ANOVA for comparison, and the results show that there is a statistically significant difference between the real and estimated values for some body parts. They claim several reasons for this difference, such as the positions of the subjects, the positions of the camera, problems with landmark identification, shape quantificatiıns, and calibration. Despite the imperfections, the authors state that the proposed system is open for further development [19].

Another similar study in 2019 leveraged 2D images of human subjects to estimate 13 different anthropometric measurements [42]. Shah et al. use two images acquired with an RGB camera located at a specific distance from the subjects in their work. This pre-determined distance is factored into the calculations while transforming the findings from pixel space to real-world metric space. In their pipeline, they use the Canny Edge Detection algorithm for locating specific bodily landmarks such as shoulders, hips, and hands. They collect two images from each subject (one anterior, one lateral), and they calculate circumferences of particular body parts like the waist and hip with the assumption that the cross-sectional area of the human body is elliptical. They calculate the girth by factoring in the widths obtained from the images. They evaluate the performance of their model by testing it on 20 subjects and share the outcomes as regression and correlation values. They conclude that even though the results are not perfect, their proposed model outperforms state-of-the-art models and has room for further development [42].

In another work conducted in 2019, de Souza et al. use CNN and other ML methods for estimating seven body parts [43]. Using a smartphone, they collect four images of human subjects from the front, back, right and left sides. In their experimental setup, the subjects wear nothing but an undergarment, and the background and lighting of the environment are configured in a certain way. The subjects are required to hold their arms at a specific angle. The height of the subject is measured manually, and the value is given as input to the pipeline so that it can be used as a reference for transformations from pixel space to real-world measurement space. After collecting the images, they perform background elimination, contouring, and key point detection algorithms. The results are used for locating the positions to measure and estimate measurements. They use different numbers of references for approximating body parts. For example, waist circumference is estimated with images from all four images, and thigh and calf are measured with three images. In the end, they present their scores in terms of mean squared errors for each body part they are interested in. They discuss that even though the results are imperfect, the system has room for further improvements [43].

In another recent work, done in 2020, Jamil et al. [48] developed a system in which they employed a Kinect camera to estimate the lengths of 13 body parts. They do not include the calculations of circumferences of any body part and use the depth perception property of the Kinect camera. In order to transform pixel values to real-world units (centimeters), they use the hand lengths of the subjects. This measurement is collected, along with other body part lengths, before the image acquisition phase of the experiment. Their camera is located at a specific distance from the subjects, and the subjects are photographed with their clothes on. They calculate the lengths of the body parts using the Kinect landmark detection model. The distance between specific landmarks corresponds to the lengths of the body parts. They present the performance of their work in terms of absolute error between the actual and estimated measurements. According to the results, average errors for each body part lie between 2.16-3.45% [48].

In another work done by Shah et al. [49], the researchers design a system intending to estimate the measurements of four regions: shoulders, chest, waist, and inseam. They collect two 2D images of human subjects, one from the anterior and one from the lateral view. They use the BodyPix body segmentation model, which TensorFlow [50] provides. They experimentally determine the locations to take measurements and pinpoint them on the images. According to their model, for example, the waist is measured 35 pixels above the hip. The exact location of the hip is detected using a body segmentation model. As a reference for transforming from pixel space to real-world distance units, they use the height of the human subject, collected before the experimentation. They test their proposed system on 50 human subjects and they present their error as the mean absolute error for each body part in focus. According to their results, for the shoulder, chest, waist, and inseam regions, mean average errors are 0.8, 2.5, 1.2, and 1.8 inches, respectively. They state the fact that the performance of the model is highly dependent on several features like the fit of the clothes the subjects are wearing, the camera position, and calibration, in addition to the performance of the body segmentation model [49].

In their work, Sheth et al. [18] use mirror selfies as input images, where the subject is in front of a mirror and holding the phone in one hand. The phone that took the picture has a significant role since the dimensions of the phone are added to the calculations as a reference for transferring the pixel values to real-world metrics. They estimate 11 body parts, 4 of which are lengths of several body parts, and the remaining 7 are circumferential regions. Their pipeline mainly contains object detection, data preparation, and measurement prediction. For object detection, they use a pre-trained faster R-CNN model from the TensorFlow object detection API for detecting the person and the cell phone on the image. They use supervised learning algorithms for measuring the body parts they are interested in. In their system, the images constitute the training data; the actual measurements are the labels. They implement 4 machine learning algorithms: k-NN, SVR, DTR, and linear regression. They test their models on 70 male subjects. The results show that DTR gives the worst results while the remaining three perform similarly, each with slightly better results for different body parts. The error rates of the models are observed to be <7%. They claim that the model has room for further development and with the additional statement that the model should also be tested on female subjects [18].

1.3 Hypothesis

A fast, simple, and accurate way of obtaining anthropometric measurements can benefit several groups, such as medical practitioners, personal trainers, and those monitoring their weight-loss progress. An automatic method can be developed rather than using traditional manual methods, which are time-consuming and prone to errors. Methods that include 3D imaging techniques yield accurate results; however, they require complex camera equipment. Several studies prove that obtaining reasonably accurate results using 2D imaging techniques is possible. Most current studies using 2D images necessitate external input variables or special environmental conditions. An accurate, portable, easy-to-use, full-automatic system without external input can be developed using the most recent image processing techniques.

2. MODELS

In the scope of this project, three pre-trained models were used. Two of them, MediaPipe (see Section 2.1) and BodyPix (see Section 2.2), constitute the main components of the proposed measurement pipeline. At the same time, one of them, SMPL (see Section 2.3), is only used for comparing the output of the proposed system with an existing commercial product. Technical details of each model are shared under corresponding sections.

2.1 MediaPipe

MediaPipe [51], developed in Google Research Lab, is a framework used to create pipelines for analyzing sensory data of various kinds, such as audio and video. Processing the input data through different components like model interface, media processing algorithms, and data transformations, it “perceives” the objects and environment on the data. Ultimately, it outputs descriptions such as object localization and facial landmarks [51].

The product is available for public use, and machine learning practitioners such as researchers, students, and software developers can employ this framework since it is an open-source model. The advantage of the framework is its speed and simple structure, which makes it adaptable to various hardware platforms, including mobile and wearable devices. Besides pre-trained pipelines, the components that make up pipelines are also available. Developers can create custom pipelines or components and include them in the pipeline [51].

Pipelines are called *Graphs* in MediaPipe. Similar to graphs used in computer science, the pipelines have nodes called *Calculators* and edges called *Streams*. The data that flow through the Graphs, *Packets*, are processed by Calculators with different jobs, and Streams transfer them [51].

In the current version, MediaPipe has solutions for tasks related to three data types [52], namely vision, text, and audio. Some examples of vision tasks are object detection, image segmentation, gesture recognition, and hand, face, and pose landmark detection. Besides, it can classify text and audio-based data.

In this project's scope, the only service used was the one related to Pose landmark detection (hereafter MediaPipe Pose). This model accepts input data in still images, decoded video frames, and live video feeds. The outputs of the model are pose landmarks in both worlds and normalized image coordinates, and a segmentation mask. It can detect 33 body landmarks shown in Figure 2.1.

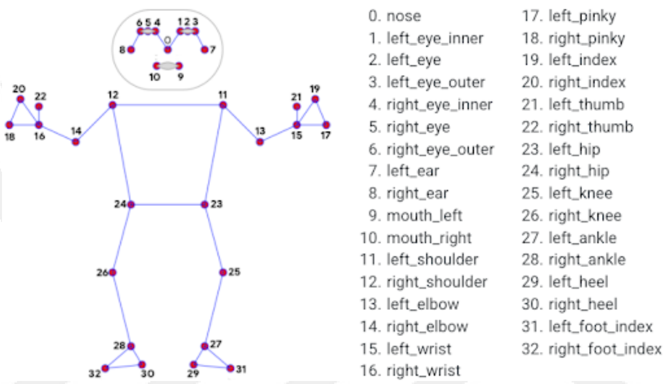

Figure 2.1 : Landmarks tracked by MediaPipe Pose [53]

2.2 BodyPix

BodyPix 2.0 (hereafter BodyPix) in TensorFlow [50] is a potent tool that can perform real-time body segmentation on humans. It detects 24 body parts even when multiple humans are in the frame. BodyPix is based on a convolutional neural network, and the designers have opted to use MobileNet [54] instead of ResNet [55] network for its lightweight. The advantage of the MobileNet over ResNet is that the former can be used in applications that need to be run on mobile devices.

Before detecting the body parts, BodyPix first applies a person segmentation which distinguishes the human body from the background. This is done by feeding an input image to the MobileNet, and the sigmoid activation function transforms the output to the range $[0,1]$. This value corresponds to the probability of one pixel belonging to the human body or not. If the value is over the segmentation threshold, the pixel is considered a part of the body. An example of the output of the BodyPix model is depicted in Figure 2.2. In the image, different colors correspond to different body parts detected by the model.

Figure 2.2 : A sample output of Bodypix [56]

A similar approach is used to detect the body parts, but this time, 24 channels, each corresponding to a predetermined body part, are used. Each pixel (u, v) is assigned to a body part based on Equation 2.1 [57]. In the equation, I_b represents the index number of the body part, $P(u, v, i)$ represents the probability of pixel at location (u, v) belonging to the body part i, and I is the list of body parts in the form $I = \{0, 1, ..., 23\}$.

$$I_b = \arg\max_{i \in I}(P(u, v, i)) \tag{2.1}$$

The BodyPix package in TensorFlow allows the developers to choose the value for the aforementioned segmentation threshold value, which determines whether a pixel belongs to a body part. This number is supposed to be between 0 and 1, and the default value is 0.5.

2.3 SMPL

The Skinned Multi-Person Linear model (SMPL) is a statistical model for human body shape and pose estimation. It is designed to represent the shape of a human body compactly and flexibly that can be used for various applications, such as computer animation, virtual reality, and body shape analysis [58].

SMPL is based on a linear blend skinning technique that models the deformation of the human body in motion. The model is constructed using a database of 3D body scans of diverse people, which allows it to capture a wide range of body shapes and sizes. The model also includes parameters for controlling the body's pose, such as joint angles and bone orientations [58].

The SMPL model has been a prominent tool in various areas, such as the clothing industry, motion capture, and gaming sector. Besides the popularity in the industry, SMPL is widely used in scientific research such as medicine (e.g., [59]–[61]), gaming technologies (e.g., [62]–[64]).

Overall, SMPL is a powerful tool for modeling the human body and has helped advance the state-of-the-art in computer graphics and vision research.

Meshcapade is a company that specializes in 3D modeling, animation, and visualization services. They offer various services, including character modeling, rigging, animation, and visual effects for industries such as film, television, gaming, and advertising [65].

The company leverages the SMPL model for their products. Among various services provided by the company, only the one related to body measurements was included in the scope of this project. This product has two modes; in the first one, the user gives some numerical inputs representing body measurements, and the system creates 3D human models, and in the second mode, the user gives 2D images of an actual human. The system outputs 3D human meshes along with body measurements. A sample output created using the latter mode is shown in Figure 2.3.

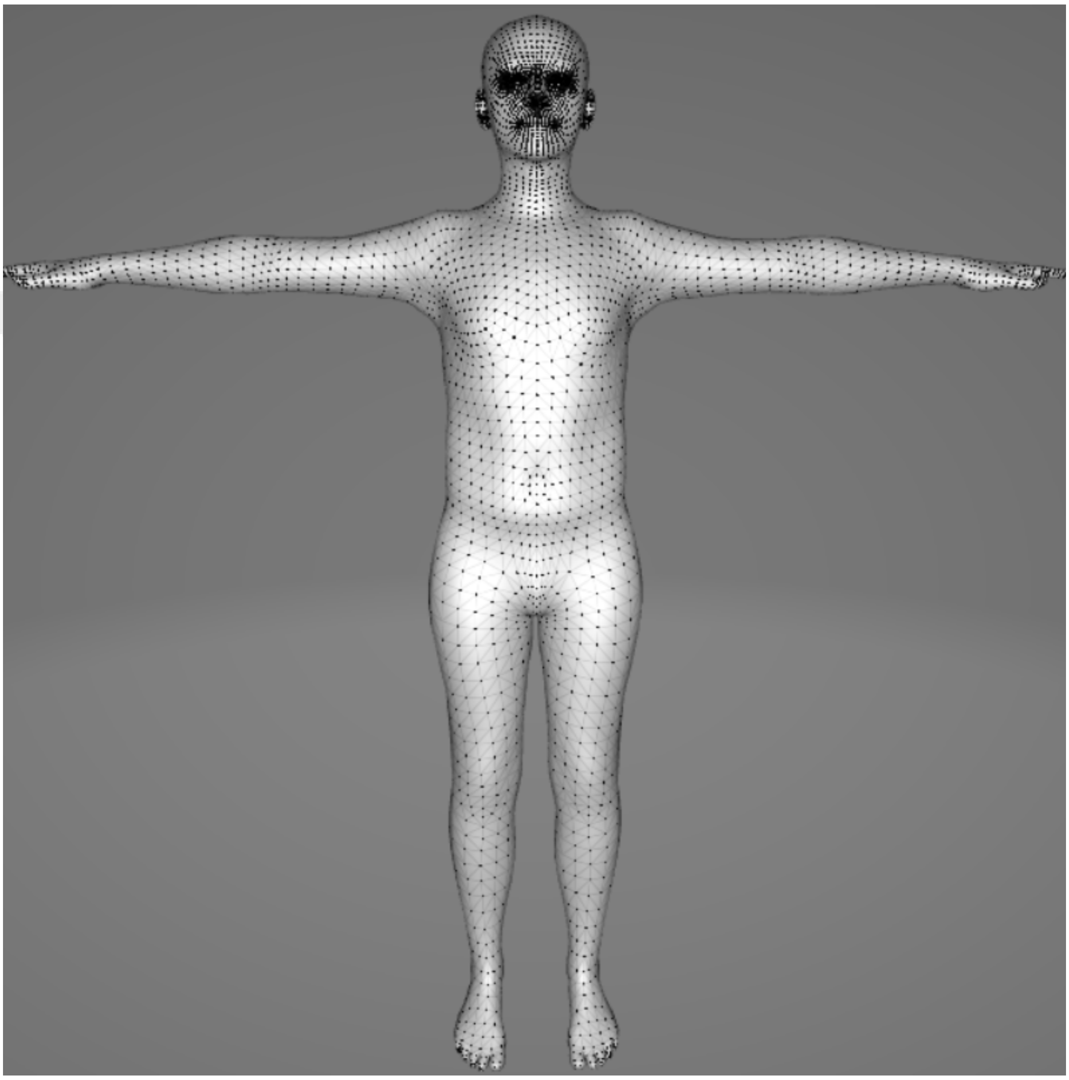

Figure 2.3 : A sample output of Meshcapade [66]

3. SYSTEM DESIGN

The proposed system has two components: hardware that collects the images from the human subjects and software that processes the images and outputs the anthropometric measurements.

3.1 Camera Setup

Hardware needed for the proposed measurement system contains two parts: a smart mobile device (i.e., smartphones or tablets) with an embedded optical camera and an attachment that carries two or more laser pointers. Laser sources are located so that they are projected to where the camera is directed. The positions of the laser pointers have great importance since if they are placed far from the camera, it becomes harder to estimate where they will be located in the image. Experiments show that the best results are taken when the lasers are located around the camera because, in that case, the laser pointers project precisely to the center of the image, which makes it easier to detect them on the software side.

In this project's scope, two camera setups are designed and tested. The first system (hereafter Version 1) is designed as a prototype in order to test the validity of the concept in mind, while the second system (hereafter Version 2) is a technologically better version of the prototype and manufactured in professional facilities by demand.

3.1.1 Version 1

This initial prototype of the system, shown in Figure 3.1, was manufactured with the help of a 3D printer. It comprises two parts: a bottom part that carries laser pointers and a top part that holds the device that takes a photograph.

The bottom part contains three different sets of laser pointers: a pair of red lasers, green pointers, and infrared laser pointers. The laser sources are aligned in a horizontal line, and the distances between the pointers of each pair can be tweaked with the help of an adjusting wheel. A metric measuring tape is attached to the bottom to measure the distance between the laser sources. The lasers are powered with a portable source like a power bank through a USB Type-C cable.

The upper part, which is attached to the bottom part, works as a mobile phone holder that stabilizes the camera while taking a picture. Because the system has no fixed machine, any smartphone with an arbitrary brand, model, or OS can be used with this system.

Figure 3.1 : Camera Version 1. Blue squares indicate the locations of laser points, green rectangle shows the adjusting wheel.

In order to take a photograph of the human subject, one pair of lasers (the current version of the software is designed for only the red lasers) should be lit and projected on the human subject, and the phone should be placed on the top part. The experiments show that when the phone is placed upside down, the accuracy of the measurements increases. This is because when the phone is upside down, the camera becomes closer to the laser points, which locates the laser points on the center of the image.

Experiments show that there are a few things that could be improved with this hardware design. One of the most significant drawbacks is that the laser pointers are not always perfectly aligned horizontally. The rails where the laser pointers are placed are not smooth, and this causes small bumps on the surface. Even though this is not noticeable in the source, the misalignment becomes apparent when projected on a distant surface (e.g., the human subject).

Another area for improvement with this design is the distance between two laser pointers. The distance between these pointers must be a fixed value for the software to work accurately. However, despite the existence of a measuring tape, it is tricky to fix this distance. For example, when the distance is set to 5cm, laser sources do not horizontally align due to the aforementioned smoothness issues on the rails the lasers are attached to. For these reasons, the design needed to be improved with better features.

3.1.2 Version 2

The second prototype solved the problem of varying distances between laser sources during the manufacturing phase. This version was produced using Computer Numerical Control (CNC) machine, which fixed the laser pointers to their locations. Since the user cannot adjust the lasers' positions, uncertain distances between laser pointers are no longer an issue in this improved version.

As seen in Figure 3.2, there are several changes in Version 2 compared to Version 1. One main difference is that in this version, the smartphone is attached to the equipment that carries the lasers. The lasers are placed around the camera, and this upgrade guarantees that the laser points on the image are located precisely in the center. Centering the laser pointers is vital because this makes the software that detects the laser points simpler by constraining the searching area to the pixels on the center window.

Another novelty of the second version is the number of laser pointers. In this version, four laser pointers are positioned to form a diamond shape around the camera. The main idea behind this upgrade is that if there are two sets of vertically and horizontally aligned lasers, there will be a different control mechanism for calculating the distance

Figure 3.2 : Camera Version 2. On the left, the whole system, including the tripod. On the right the camera and laser setup. Blue squares show the laser points, the red square shows the location of the camera.

between lasers. In other words, if the system suspects that the horizontal lasers are misaligned somehow, it can use the projections of the vertical lasers.

The lasers used in this version are significantly dimmer than the lasers of the first version. However, it must be powered externally via a USB Type-C cable. The smartphone is an Android device running on Android 9 and has a camera with 20 MP. Since the software that processes the images is yet to be in the form of a publicly available application, the photographs taken by the camera must be sent to a digital device (like a PC) to be processed. The smartphone is equipped with the necessary connection properties and can send photographs via an Internet or Bluetooth connection.

Even though the laser equipment and the case that holds everything together put some extra weight, it is easy to hold and carry the device. However, the experiments showed that attaching the device to a tripod is a better approach since any camera movement lowers the image quality and results in high measurement errors.

3.2 Software

The photographs of human subjects, which are collected using the camera setups mentioned in Section 3.1, are fed to a software that has been custom designed for the purpose of estimating four anthropometric measurements, namely height, girths of bust, waist, and hip. Figure 3.3 depicts the system's pipeline of the whole system, starting from feeding thee input to obtaining the measurements.

Two photographs of the human subject, one in anterior and one in lateral view, constitute the pipeline inputs. In the first step, landmarks of the human body are determined using the pose estimation model, whose details are shared in Section 3.2.1. Following the pose estimation, both images are fed through the body segmentation model (for details, see Section 3.2.2). The outputs of pose estimation and body segmentation models are leveraged while spotting the locations of the body parts that will be measured. The widths of the body parts are calculated using algebraic operations. After obtaining the widths of the specific body parts, the laser point projections on the images are detected. With the help of the prior information on the distance between the laser points, the widths are transformed into the metric system (specifically, to centimeters). The girths of the body parts are estimated under the assumption that the cross-sectional area of the human body converges to an ellipse. The subject's height is estimated using only the lateral view of the subject. Each component of the given pipeline is explained in detail under designated subsections.

Python programming language was selected for image processing applications and web-based interfaces for user interaction. For the purposes image processing, OpenCV [67], TensorFlow [50], Matplotlib [68], Pandas [69], and NumPy [70] libraries are used. For web-based interface, Flask [71] framework was preferred.

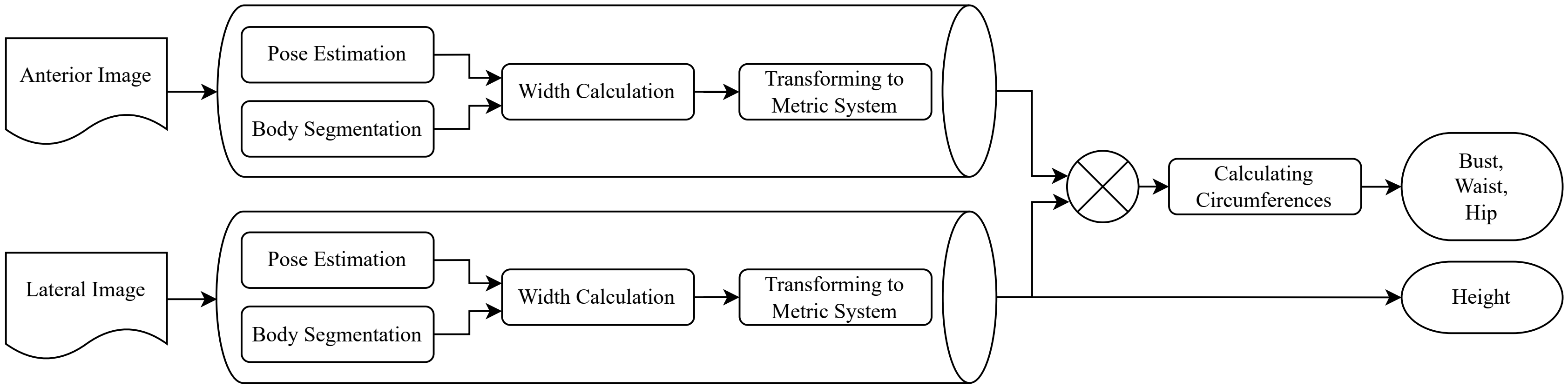

Figure 3.3 : Pipeline of the software system.

3.2.1 Pose estimation

Measuring body parts using an image requires two steps: locating the body part to measure and taking the measurement. For locating the relevant body part, some reference points on the body can be used. This is where a pose detection model becomes a necessity.

In the application, the pose estimation model of the MediaPipe Pose framework has been used (see Section 2.1). This model estimates the pose of the human body on an image in real-time. The model can detect 33 pose landmarks, including features of the face, hands, feet, and torso. However, only four of these landmarks sufficed to locate the body parts focused on this project's scope. By spotting the shoulders (left and right) and the hips (left and right), it is possible to estimate the bust, waist, and hip positions.

The input image is fed to the model to find the pixels that represent the shoulders and the hips. The model outputs pixel coordinates as an array of arrays in which the indexes represent the body part identification number, and the values contain the coordinates of the corresponding pixels. This result is passed to the following components of the pipeline.

3.2.2 Body segmentation

The body segmentation model used in the proposed software, BodyPix 2.0 (see Section 2.2 for details), can determine 24 distinct body parts. In the current version of the proposed measurement system, only 12 are used, including the parts of the torso, arms, legs, and head.

When the model is run on the input image, it processes it and returns a mask that is indexed and color-coded based on the body part. The pixels that belong to the same body part are grouped and represented with a specific color and an index number. The index number is used for random access to pixels that belong to a specific body part, and the colors are an essential part of the visualization.

The success of the whole measurement system is highly dependent on the body segmentation model. If the model does not detect a body part that has a critical role in measurements, the whole system aborts with a failure. Hence, it is crucial to tune the model's hyperparameters to find critical body parts and fit the body as perfectly as possible.

As stated in Section 2.2, the model has a hyperparameter that determines the threshold for belonging to a body region. Even though the default value is 0.5, the experiments showed that setting this parameter to 0.8 gives better results. Higher values result in tighter regions that compensate for possible errors caused by the loose clothes the subject is wearing.

The mask obtained from this model constitutes the basis of all subsequent calculations on the pipeline.

Figure 3.4 depicts masks created by the aforementioned pose estimation (see Section 3.2.1 and body segmentation models.

Figure 3.4 : Sample input images and the masks created by the pose estimation and the body segmentation models.

3.2.3 Width calculation

As previously mentioned, initially, the related body parts must be spotted on the image to calculate the width of a body region. Landmarks obtained from the pose estimation model (see Section 3.2.1) and body parts obtained from the body segmentation model (see Section 3.2.2) are leveraged for spotting the regions. After determining the measurement's location, the matrix containing the pixel coordinates of each body part is used for calculating the width of the specific body part on the image

3.2.3.1 Bust region

The pose estimation model, MediaPipe Pose, does not provide a landmark to locate the bust area. Hence, only the body segmentation model, BodyPix, is used for determining the location for measuring the bust circumference. Experiments show that the bust roughly falls onto the torso part, which starts right after the region for the arms finishes. Since the human subjects open their arms wide open (in T-shape) in the input images, locating where the arms end is not challenging.

However, since human subjects cannot hold their arms in a straight line, the positions where the arms end at each side differ. Rather than considering one specific arm or averaging the positions where both arms end, it was preferred to do the calculations based on the arm that is lower than the other. According to the experiments, this is a good approach for the anterior images. For lateral images, it is a fact that only the subject's right arm can be seen. Hence, only the location where the right arm finishes and the torso starts is taken into consideration.

After determining the position to take the measurement, the pixels of the torso at that region are extracted, and the width of the bust is considered to be the width of the torso on the specific horizontal region.

3.2.3.2 Waist region

Waist circumference is a good metric for assessing someone's tendency for cardiovascular disease and obesity [72,73]. However, there has yet to be a consensus among the medical communities about the protocol for measuring waist circumference. There are different approaches to the measurement process. One of the popular approaches focuses on the bony landmarks (iliac crest, last rib, or midpoint). In contrast, the others use external landmarks (minimal waist, largest abdominal circumference, umbilicus, 1 cm above umbilicus, or 1 inch above the umbilicus). The choice of the location changes the overall measurements [74]. In their study, Ross et al. examine if different preferences affect the result of mortality and morbidity estimations. Their results show that it is better to use a bony landmark; hence using a midpoint or iliac crest is superior to the other methods. The comparison of the aforementioned two methods suggested no statistically significant difference in the success of the two methods in determining mortality and morbidity rates [74].

The landmarks obtained by MediaPipe Pose are neither directly related to the waist nor is there an implication of the iliac crest. Shoulder and hip landmarks are the only landmarks useful while spotting the waist region. Hence, it was opted to use the midpoint between the subject's shoulders and hip. For finding the midpoint from the landmarks, first, the midpoint of the shoulders on the horizontal axis is found, then the same calculations are applied to the hip landmarks. Finally, the vertical midpoint of these regions is obtained by a simple averaging operation.

After spotting the region to measure, the pixels that are determined to be representing the torso are used to calculate the width of the waist. For both anterior and lateral images, the same operations are applicable. When the values from both images are collected, they are sent to the next step in the pipeline.

3.2.3.3 Hip region

The pose detection algorithm employed, MediaPipe Pose, has landmarks dedicated to the left and right hips. However, the experiments showed that these landmarks are only sometimes aligned on the horizontal axis due to several factors, like minor errors in the model or the poor positioning of the camera which took the photograph. Hence, it was preferred to find the midpoint of the left and right hips on the horizontal axis. With this calculation, it becomes possible to estimate the location of the hip on the horizontal axis.

The second step after spotting the location that will be measured is to find the body's width in that region. BodyPix does not have a region dedicated to the hip area. Experiments show that the hip region can be contained in pixels that are a part of the left and right legs and torso. By merging those groups, the system is guaranteed to find the pixels representing the hip.

The last step of finding the hip's width is to count the number of pixels between the leftmost and the rightmost borders of the hip. A simple subtraction operation between pixel coordinates can do this.

As mentioned earlier, the method applies to both anterior and lateral images. When the calculations are completed, the values are sent to the next component on the pipeline.

3.2.3.4 Height

The subject's head and feet must be visible in the image to measure the height. Both the anterior and lateral images have this property. However, the experiments show that the body segmentation model, BodyPix, fails to fully detect feet on the anterior images due to perspective issues. Hence, it gives more accurate height measurement results when only lateral images are used.

Compared to the other anthropometric measurements, calculating height is simpler since it only requires one photograph, and the only thing that needs to be done is a simple subtraction operation between the vertical position of the highest and the lowest pixels on the human body. In theory, the top-most pixel on the human subject belongs to the head, while the bottom-most pixel belongs to the feet of the subject. Since BodyPix provides labels for these body parts, it is easy to locate them. After obtaining the distance between the head and the feet, the value is sent to the next component of the pipeline.

3.2.4 Transforming to metric system

The values collected by the procedures mentioned in Section 3.2.3 are not in standardized metrics but in pixel values. However, a measurement is meaningful if it is given in a standard form, like meters.

Switching to meters (or centimeters) from pixel widths is effortless if the transformation constant is known. In other words, it is crucial to know how many centimeters the distance between two pixels correspond to.

This information can be acquired in different ways. During the phase of taking the photographs, the place where the human subjects are standing can be pre-determined, and this way, the distance between the subject and the camera can be fixed. Consequently, the pixel-to-meters transformation can be quickly done by considering the camera's resolution.

Another method to obtain a transformation constant requires a scaling object for geometric reference that can be seen on the image, such as the scales used in forensic photography [75]. Based on known distances on the image, this method can transform all the distances into real-world units (like meters).

In the proposed method, the second approach is employed, and rather than putting a geometric reference scale on the image, laser pointers are used. The distance between two laser pointers is known *a priori*. Hence, considering this fixed value between laser pointers, which the light source has determined, and the number of pixels between projected laser points, the transformation between pixels and centimeters is done.

One of the crucial steps of the process is to detect the laser projections on the image. This step constitutes the heart of this stage because if the laser points are not detected, the execution of the program is terminates with failure. Another feature that highly affects the system's performance is accurately determining the distance between the laser points on the light source. Positioning the lasers inappropriately around the camera results in high errors in the final measurements.

3.2.4.1 Detecting laser points

As mentioned in Section 3.1, two camera setups work with different laser characteristics. Even though the positions and the number of laser sources are different on each version, it is not necessary to develop two distinct algorithms to detect laser points projected on the images taken with both machines. Hence, only one algorithm has been developed, whose input is the raw image taken with the aforementioned camera setups, and the output is the pixel coordinates that represent the laser points on the image.

As mentioned in Section 3.1.2, camera setup version 2 is designed so that the laser points fall on the center of the image. For camera setup version 1, even though the hardware does not guarantee the laser points are located in the center of the image, during the phase of collecting the image, the user can position the smartphone so that laser points are roughly located in the center of the image (see Section 3.1.1 for details). Considering this, the algorithm is designed to only focus on a center window that has been cropped from the original image. Experiments show that cropping the image to 10% of its size is enough to contain the laser points on the image. Then a thresholding operation based on the redness of the pixels is done on the cropped image. Because the laser points are red, this thresholding mostly eliminates the pixels unrelated to lasers. However, some pixels that belong to the human subject, such as clothes or jewelry, may still be present in the image. Hence, more operations are needed to get rid of those unwanted pixels.

In the second part, the image is converted to gray scale and another thresholding that considers the intensities of the pixels is executed. Since laser points are bright with respect to other pixels, this operation mostly deletes pixels that do not belong to the lasers. By assumption, the resulting image should contain only the laser points. However, the experiments showed that sometimes, due to the lighting issues, the texture, and the color of the clothes the subject is wearing, some additional pixels may still be present on the image. This is why a final step is needed before obtaining the laser point locations.

An image-closing operation is applied to the remaining pixels to wipe out the small holes that the laser pixels may have. This also merges some scattered pixels that managed to live to this point. Resulting pixel groups, hereafter blobs, are checked for some conditions, such as the size, morphology, and location. The blob is deleted if it is too big or small, if it is too close to any of the borders of the image, or if it does not have a circular shape. Hopefully, the resulting blobs belong to the laser points on the image. The algorithm returns the pixel coordinates of the centroids of the blobs that belong to the laser points. The flowchart of the algorithm is depicted in Figure 3.5.

Even though they are mostly similar to each other, two algorithms were designed to process the images collected from two proposed camera setups, separately.

The first camera setup has two laser points. Thus, the algorithm mentioned in Section 3.2.4.1 returns the coordinates of two pixels. Assuming that the lasers are horizontally aligned, the distance between these pixels is calculated by subtracting vertical coordinates. The correspondence of this value to the metric system depends on the machine's calibration. The value calculated is then sent to the next component on the pipeline.

The second version of the camera setup has four lasers in a diamond shape around the camera. In theory, with these four lasers, the calculations would be more accurate because, this time, there would be more references to rely on. However, experiments showed that one of the lasers (the right-most one) is not as bright as the others, and it is not fully seen on the images of human subjects. This eliminates the pixels of this laser point during one of the stages of the laser detection algorithm, and the resulting list has coordinates for three laser points rather than four.

Despite missing one laser point, it is still possible to determine the coordinates of the laser points. However, the algorithm sometimes fails to detect all of them due to lighting and camera angle issues. Among the three laser points (top, bottom, and left), the distance between them is used as the reference if the top and bottom layers are detected. According to the design of the equipment, the distance between left-right

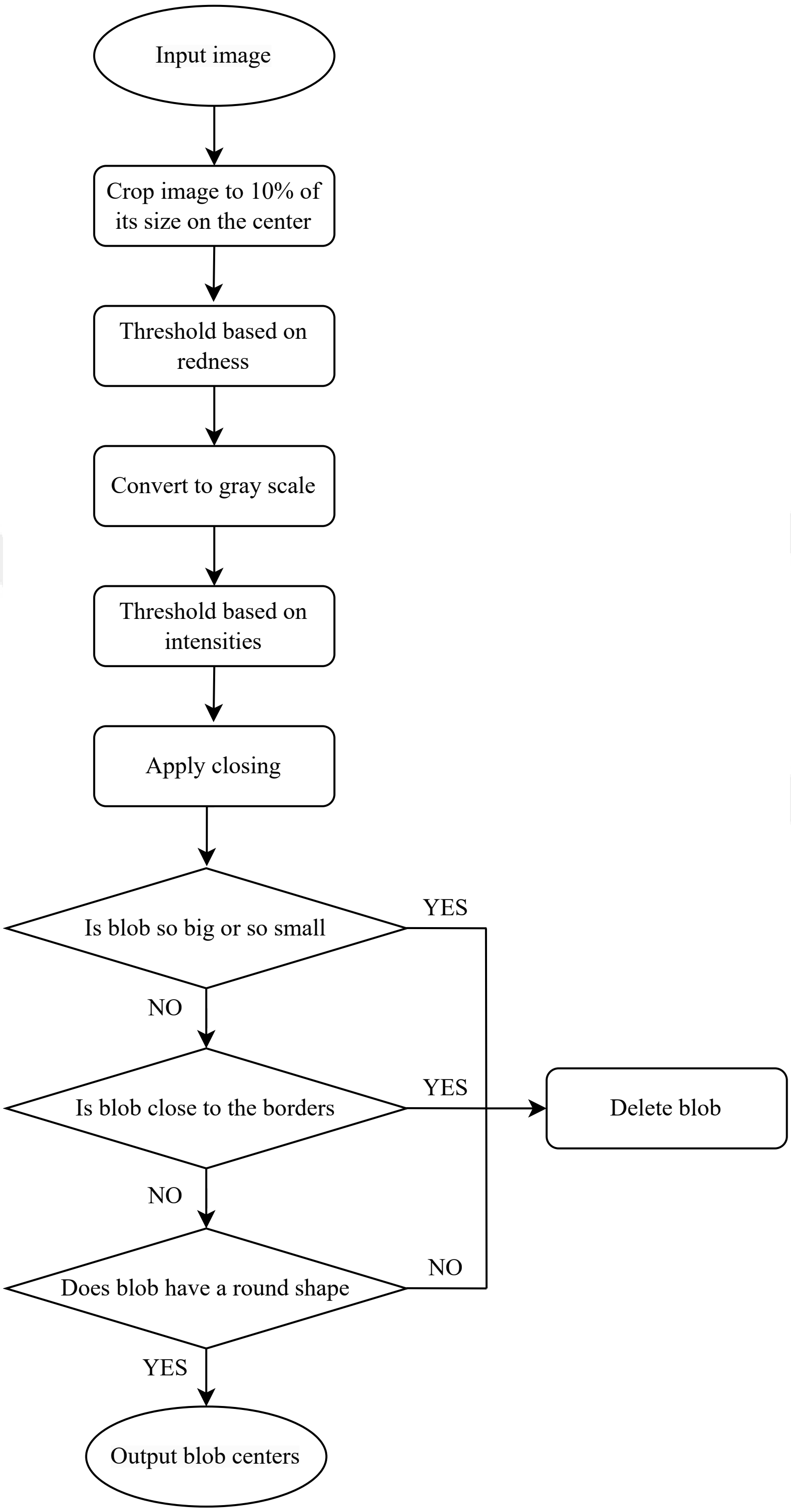

Figure 3.5 : Flowchart of the laser detection algorithm.

and top-bottom pairs is 5cm. If one of the top or bottom is missing, and the left one is present, then the distance between the left laser and the top or bottom is considered. This distance can be calculated as 3.53 cm using the Pythagorean theorem. The calculated value is then sent to the next step of the pipeline.

3.2.4.2 From pixels to centimeters

After extracting the pixel distance between the laser points, the next step is to combine this information with the distance in the laser light source to obtain a transformation constant. This reference will transform every distance on the image from widths in pixels to widths in centimeters. This simple algebraic calculation uses Equation 3.1. In the equation, c_t represents the transformation constant, d_k is the known distance between lasers on the light source, and this term is in centimeters, d_l is the distance between laser points projected on the image, and this term is in pixel units.

For camera setup version 1, d_k is set to 5.5 cm, and for camera setup version 2, this value is 5 cm by design.

$$c_t = \frac{d_k}{d_l} \tag{3.1}$$

The resulting transformation constant c_t transforms distances in pixel units to centimeters throughout the image. Equation 3.2 gives the operation needed for transformation. In this equation, c_t represents the transformation constant calculated with Equation 3.1, d_x is any distance on the image in pixel units, and the result d_c is the distance in centimeters.

$$d_c = c_t d_x \tag{3.2}$$

It should be noted that transformation constant c_t is specific to the image, and it needs to be calculated for every image, including the anterior and lateral images of the same subject. Even though the subject is the same and the images are taken consecutively; every little movement of the subject changes the transformation constant, thus changing the measurement results.

Finally, in this pipeline component, the widths of the body parts are transformed into centimeters and sent to the next step of estimating the circumferences.

3.2.5 Estimating the measurements

3.2.5.1 The height

As mentioned previously, the height is measured using only the lateral image. The height in centimeters is reached after the transformation step explained in Section 3.2.4.1 with no further calculations.

3.2.5.2 The girths of bust, waist, and hip

In the physical world, a measuring tape is wrapped around the corresponding locations to measure the body parts we have focused on (namely, bust, width, and hip). However, in the digital world, where 2-dimensional images are the only inputs, a new approach is needed for taking the measurements. For this purpose, it is assumed that the cross-sectional areas of all these body parts, the bust, waist, and hip, are elliptical, and the girths of these body parts correspond to the circumferences of these ellipses.

As shown in Figure 3.6, an ellipse has two axes: major and minor. According to the aforementioned assumption, the width obtained from the anterior image constitutes the major axis of the ellipse. Similarly, the width gathered from the lateral image constitutes the minor axis. Figure 3.7 depicts an example of locating the major and minor axes of the ellipse on the anterior and lateral images.

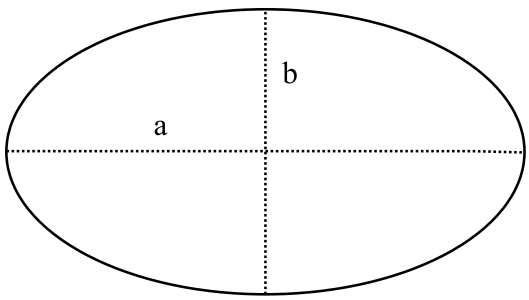

Figure 3.6 : Major (a) and minor (b) axes of an ellipse.

The circumference of an ellipse is calculated using Equation 3.3 where *a* is the major axis, *b* is the minor axis of the ellipse, and *C* is the circumference.

Figure 3.7 : Major (on the left) and minor (on the right) axes of the assumed ellipse on the human subject.

$$C = 2\pi\sqrt{\frac{(\frac{a}{2})^2 + (\frac{b}{2})^2}{2}} \tag{3.3}$$

Calculating the circumference of the ellipse, whose major axis is the width obtained from the anterior image and the minor axis is the width obtained from the lateral image, using Equation 3.3 is the last component of the whole pipeline. The output of the calculation is the girth of the body part in focus, namely, the bust, waist, or hip. The unit of the resulting value is centimeters.

4. EXPERIMENTS

Assessing the performance of the proposed system is possible with testing on actual humans. For this purpose, an experiment was designed, which included the proposed camera setup and the software that performs the calculations on the collected images.

The experiment is designed to evaluate the system's performance as a whole. That includes not only the measurements' accuracy but also the system's reaction to different environmental situations, such as lighting, background, and the clothes the subject is wearing.

The main aim of the experiment is to collect images of several human subjects with the proposed camera setups and process the images with the proposed software to obtain measurements automatically. The accuracy of the results would be assessed by comparing the automatic results with actual measurements of the subject, which are collected by traditional manual methods.

For a further analysis of the proposed model, a commercially available product that creates 3D models from 2D images of human subjects is used. The model (see Section 2.3 for details) can estimate the measurements of the human subject after creating a 3D body model. Since this model is trendy in the industry and the academic communities, it was preferred to compare the proposed model with this existing product.

4.1 Experiment Setup

The steps included in the experiments are as follows:

- Preparing the camera equipment,
- Preparing the subject for photographing,
- Taking photographs with proposed camera settings,
- Measuring the body of the subject with traditional manual methods,

- Feeding the photographs to the proposed software,
- Comparing the output of the system with real values.

4.1.1 Preparing the subjects

One of the proposed system's goals is to work accurately when the human subject is fully dressed. It was also aimed to design a model that works accurately independent of the color or the drape of the clothes the subject is wearing.

Initial experiments conducted during the prototyping phase showed that if the human subject is wearing loose clothes that do not fit their body, the pose estimation model manages to locate landmarks; however, the body segmentation model fails to detect the body parts successfully. Instead, it incorrectly marks pixels that belong to the cloths as body parts. Hence, it was preferred to take action before photographing the subjects to eliminate the errors that may occur due to this weakness of the body segmentation model. Tightening the top garment on the subject using a peg is an easy solution that does not require too much effort. Before taking pictures, if the subject wore a loose blouse or t-shirt, it was tightened from behind. If the garment was already tight, no action was taken.

Another vital intervention in the subject's clothes was related to their garment color. Early experiments showed that because camera setup version 2 contained relatively dim lasers, the lasers were not seen on the image if the subject wore dark colors. To ensure that the software detected the laser points, a white piece of paper was attached to the cloths of the subject to where the lasers were projected. The results show that this method works on subjects wearing dark clothes, but if the subject is wearing light colors, there is no need for paper as light colors reflect the laser lights properly.

4.1.2 Collecting images

In order to test both of the aforementioned camera setups, each subject was photographed individually using two of the machines. The subjects were first prompted to stand in a T-shape for pictures of the anterior view, and then, they were told to turn to their left (manifesting their right side to the camera) and hold their arm in front of them, like in a horizontally flipped L shape for the lateral view.

The images collected were stored in the devices during the experiment, and after the experiment, they were sent to the machine on which the software was executed.

4.1.3 Measuring subjects manually

The actual measurements of the subjects are needed to compare the results obtained from the proposed model with the actual values. The measurements of the subjects were collected with the help of a standard measuring tape. The measuring tape is wrapped around the related body part to measure waist, bust, and hip circumferences. The height is also measured using a tape measure while the subject is in an erect position. All results are stored digitally to be used during the performance evaluation phase.

4.1.4 Processing the images

After data collection, the images are brought together and fed to the software mentioned in Section 3.2. Numerical output, representing the height and the circumferences of the bust, waist, and hip, are stored in a spreadsheet along with the measurements of the subjects gathered manually.

4.1.5 Evaluating the performance

The absolute error of the estimation determines the performance of the proposed system. Equation 4.1 is used to calculate the relative error. In the equation, m_M represents the measurement taken manually, m_A represents the measurements estimated automatically by the proposed software, and E_r is the relative error between these values.

$$E_r(\%) = \frac{|m_M - m_A|}{m_M} \times 100 \tag{4.1}$$

4.2 Environment

Theoretically, the system was designed to be robust under environmental changes, such as different backgrounds and lighting conditions. This system feature can be checked by feeding the software with input images collected under different environmental conditions. This is why the images included in this experiment have been taken in three different rooms with various lighting and background conditions. The comparison of the results is shared under Section 5.

4.3 Experiments with SMPL

Experiments that included the SMPL model were conducted independently from the experiments done for testing the proposed model. However, the same images (anterior and lateral) were used to test the performance of SMPL. The images were uploaded to the online web application provided by the company named Meshcapade [65]. The application is open to public use, and the product is accessible by signing up to the system.

The service provided by Meshcapade can create 3D avatars from given measurements or generate 3D models of human subjects from 2D images provided by the user. The feature included in this project's scope is the one that generates 3D avatars from 2D images.

The application takes at most four images of a human subject and returns a 3D model of the subject as an object file. If the user wants, they can access the measurements of the 3D model created and download both the object file and the measurements.

The system outputs fifteen anthropometric measurements, such as height, weight, girths, and lengths of several body parts. In the experiments, we used four of these: height, girths of bust, waist, and hip. Quantitative results are shared in Section 5.

5. RESULTS

5.1 Data

In total, 19 human subjects (4 women, 15 men, all of them in their twenties) agreed to participate in the experiments. The experiments are done in three locations with different backgrounds and lighting conditions. However, due to the subject's time limitations, it was impossible to photograph them at each location. Hence, every subject is photographed once.

Early experiments showed that every detail, like the subject's position, breathing cycle, or minor tweaks on their clothes, affects the system's output. To obtain a more accurate estimate, it was preferred to take at least two photos of the subject while they were posing for the camera. In other words, except for some exceptions, there are four images of each subject, two of which are from the anterior view and two from the lateral view.

Before evaluating the experiment results, analyzing the ground truth values (manual measurements) is vital. The distribution of each data group (individual body parts) is shown in Figures 5.1 and 5.2. Figure 5.1 shows a boxplot of the manual measurements and Figure 5.2 depicts the histograms of data for each body part.

5.2 Experiment Results

Even though 19 subjects were photographed, for some subjects, the proposed systems failed to detect the measurements. The main reason for this failure is environmental. The place where these images were collected was very bright, and the subjects stood under a bright light source. The proposed model failed to detect laser points on the subject because the subjects' clothes reflected the environmental light beside the laser's lights. Hence, the model's laser detection component failed, which was a crucial step of the pipeline.

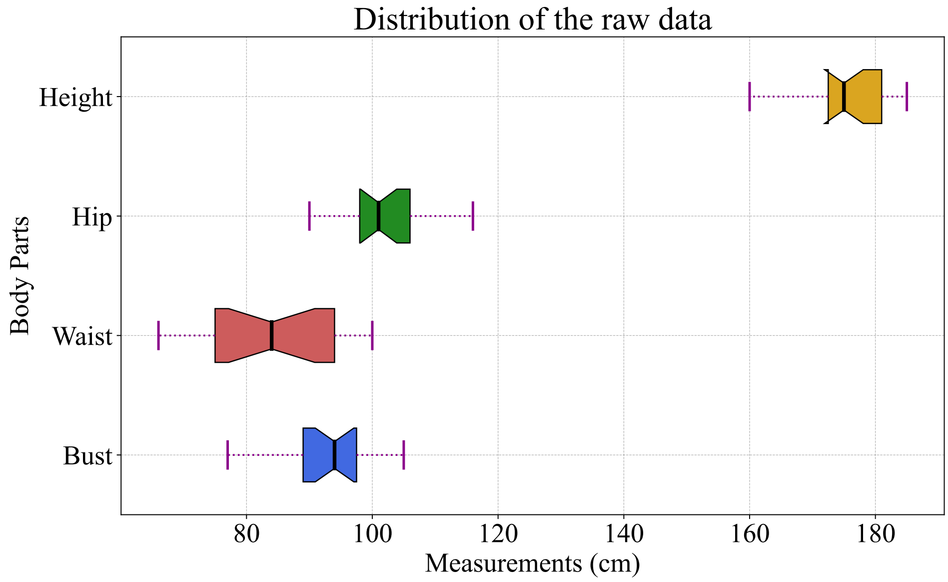

Figure 5.1 : Box plots of manual measurements

The results of the experiments, whose details are explained in Section 4, are shared in the corresponding sections. The average errors of each method are shown in Table 5.1. The accuracy rates of the models are depicted in Figure 5.3.

Table 5.1 : Average errors for body regions that were measured

	Bust Error	Waist Error	Hip Error	Height Error
V1	7.32%	9.7%	7.12%	5.0%
V2	15.9%	9.92%	2.01%	4.43%
SMPL	7.8%	10.69%	12.43%	3.33%

5.2.1 Bust circumferences

Circumference of the bust of each subject is calculated using the method explained in Section 3.2.3.1.

Bust circumferences of 13 human subjects out of 19 were calculated using the images collected with camera version 1. For the remaining 6 subjects, obtaining a result was impossible due to the environmental issues related to the lighting conditions. Considering these failures, the success rate of the system is 68.42 %. However, it should be noted that those failed input images are mostly captured under the same environmental conditions.

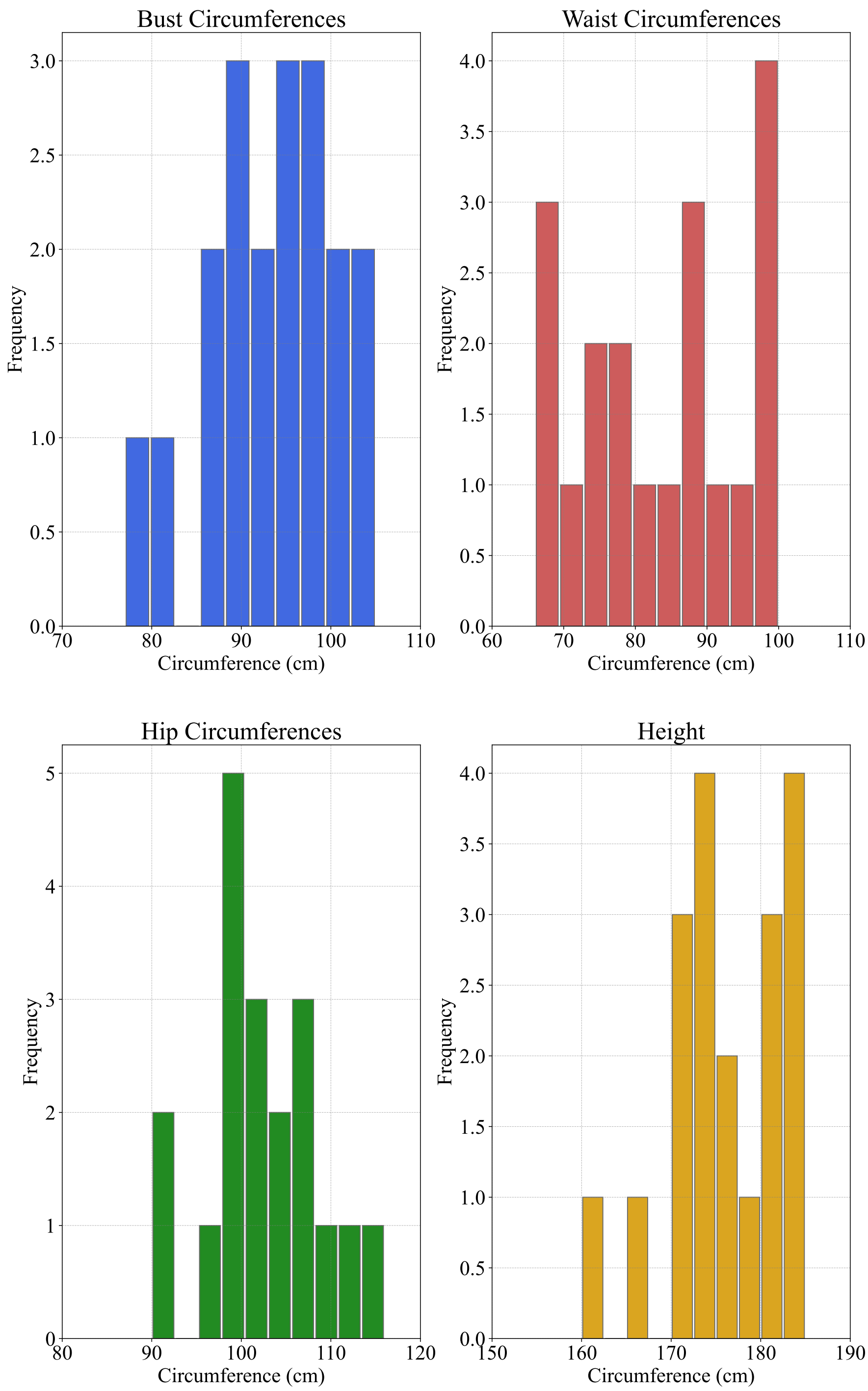

Figure 5.2 : Histograms of manual measurements

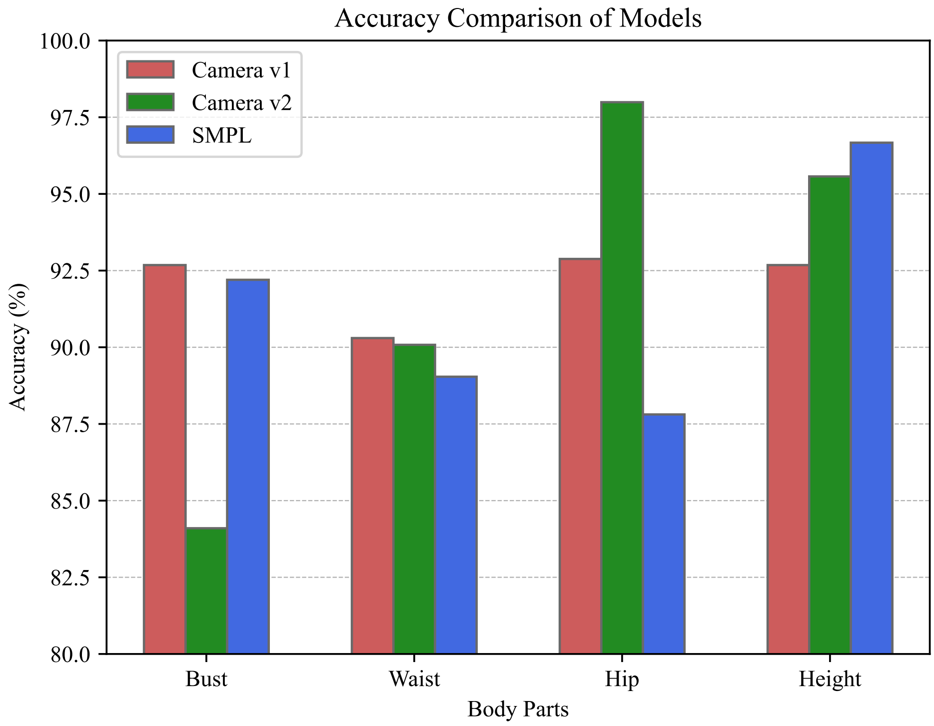

Figure 5.3 : Comparison of accuracy rates of the models.

Table A.1 shows the real bust circumferences of the subjects collected using traditional manual methods and the estimated values obtained by the proposed system. It must be noted that for subject number 12, the system failed to measure the bust circumference for the second set of images due to the problems caused by lighting. Therefore, only one measurement error was added to the overall error calculation. According to the results shared in Table A.1, the average error of the model is 7.32%.

As seen in Table A.2, for images collected with camera version 2, twelve out of 19 images were processed. Due to environmental lights and the clothes the subjects were wearing, 6 of the cases caused failures. This makes the success rate of this system approximately 63.15%. The average error for this camera setup is 15.9%.

Finally, as mentioned in Section 4.3, the images were fed to the SMPL model for comparison. The results of this model are shared in Table A.3. The model gave results for all 19 subjects. Considering the fact that this is a commercial product, this result is not a surprise. Despite this success, the error rate of this model is calculated as 7.8%.

Burst girth is a tricky region to measure. The main reason for this lies in the human anatomy. When a person breathes in air, the bust gets more prominent as the air fills the lungs, and while breathing out, the air goes out and causes the bust region to shrink. This movement can cause 2-3 cm changes throughout the breathing cycle. It should be noted that this movement is not a problem only for automatic measurements but also causes problems for manual measurements.

When the aforementioned problem is considered, it is expected to have large error percentages for bust measurements. However, it is essential to note that the source of the error may not be the proposed system, rather it may be caused by a measurement error while collecting actual measurements with traditional manual methods.

Despite the challenges, the model's error rate created with the images collected by camera version 1 seems acceptable. The big difference between the results of camera versions 1 and 2 might be due to the laser points used as reference. Even though version 2 was an upgraded version of version 1, the results related to bust circumferences show that it could have been more successful than planned.

The error rate of the SMPL model is considerably close to the results obtained from camera version 1. If this commercial model is taken as a reference, it can be concluded that the proposed model is successful.

5.2.2 Waist circumference

Like the bust circumferences, camera version 1 measured 13 subjects out of 19. Table B.1 presents the actual waist circumferences of the participants measured using conventional manual techniques, along with the approximate values obtained through the suggested system. It is essential to mention that, in the case of Participant 12, the system encountered difficulties in measuring the waist circumference for the second set of images due to lighting issues. Consequently, only one measurement error was included in the overall error calculation. As indicated in the findings presented in Table B.1, the average error of the model is 9.7%.

As indicated in Table B.2, twelve of the 19 images captured using camera version 2 were successfully processed. However, due to factors such as environmental lighting conditions and the clothing worn by the subjects, six cases resulted in failures. This implies that the overall success rate of the system for this particular camera setup is approximately 63.15%. Additionally, the average error observed for this camera configuration amounts to 9.92%.

Lastly, as described in Section 4.3, the images were also inputted into the SMPL model for comparison. The outcomes of this model are presented in Table B.3. The average error of this model is calculated as 10.69%.

When all results are compared, it can be deduced that all models yield a similar error rate, and no model significantly outperforms another. If the SMPL model is considered a reference, since it is already a commercial product, it can be claimed that both suggested methods are successful.

Another deduction that can be made from these results is that the location where waist circumference is being measured is suitable for this project. Considering the methods mentioned in the medical literature, incorrectly chosen locations could have given high error rates.

5.2.3 Hip circumference

Using camera version 1, 13 out of 19 subjects were measured, since for the rest 6, the system failed to detect laser points on the images. Since this is one of the crucial components of the pipeline, if they are not detected, the system cannot measure the body parts. Therefore, the error calculations are performed using 13 subjects. Table C.1 presents the findings for hip circumferences. On subject number 12, only one set of images was processed because the lighting was problematic for the other set, and the system did not find laser points on the image. The average error of this model is calculated as 7.12%.

The findings obtained by the camera version 2 are shared in Table C.2. The model managed to measure 12 subjects out of 19. As previously mentioned, the failed cases were due to environmental lighting issues. Despite the success rate 63.15%, the model has an error rate as low as 2.01%. With this rate, it can be deduced that there is a considerable upgrade compared to the previous camera version.

Surprisingly, the third model, SMPL, has a relatively high error rate of 12.43%. The results for each subject can be found in Table C.3.

When all the models are compared, camera version 2 has the highest accuracy while SMPL is approximately 6 times worse than the proposed model. This is an unexpected result since it was assumed that as a commercial product, SMPL would give the best results for every body part.

A possible reason for this difference might be due to the clothes worn by the subjects. The experiments showed that the body segmentation model, namely BodyPix, can mostly deal with loose clothes. However, SMPL tends to fit the clothes rather than the human body. The images created by the model seem to have a problem fitting to the area below the waist. This vast error gap might stem from this fitting issue.

5.2.4 Height

Using the images captured with camera version 1, only 11 measurements were taken out of 19 subjects. The reason for this lower number compared to the previously mentioned body parts is that the body segmentation model, BodyPix, failed to find the head for some subjects. A possible source of the problem might be the camera angle. During the step of collecting images, the camera was not centered, and for some subjects, the camera was pointing at a location lower than the hips. This caused a perspective problem, and even though the head of the subject was visible in the image, the model could not locate it. The results of the model for each subject are presented in Table D.1. The average error of these calculations is 5.0%.

As in the case of camera version 1, version 2 also successfully worked on 11 subjects out of 19. A similar perspective issue occurred in this version. Quantitative findings are shared in Table D.2. Based on these results, the average error is calculated as 4.44%.

Lastly, when the images were fed to the SMPL model, it managed to measure the heights of all subjects. The results for each subject are depicted in Table D.3, and the average error turned out to be 3.33%.

When comparing all the models to one another, it is obvious that in the results gathered from the SMPL model, the error is the lowest, which makes it the best model for estimating height. However, the difference could be more dramatic, and other proposed models also manage to estimate a subject's height.

On the other hand, the fact that, in some cases, the suggested models fail even to output a numerical value for the height makes the SMPL model more advantageous. Nevertheless, considering the failures of the models stem from environmental factors, the success rates of the proposed models can be increased by regulating the surroundings before collecting the images.

6. CONCLUSIONS

In this study, a system was proposed and tested to estimate anthropometric measurements such as a human subject's height, bust, waist, and hip circumferences using only two 2D images. The proposed system consists of a customized camera setup and image analysis software. The camera setup includes a smartphone with four laser markers and a tripod. The image analysis software is designed as a web-based application.

The system's operation is as follows: Firstly, the images are fed into the software, and the positions of body parts are determined. Then, the width of a specific body part in both images is calculated, and the pixel widths are converted to physical units. Finally, the circumferences of body parts are estimated.

Experiments were conducted on 19 human subjects. The actual measurements of the subjects were obtained, and the relative error percentages were calculated by comparing them with the predictions of the proposed model. According to the experimental results, error rates were determined for height, bust, waist, and hip circumferences predictions.

The experiment was conducted on 19 subjects (4 females and 15 males). The results show that the average relative errors for height, bust, waist, and hip circumferences are 4.43%, 15.9%, 9.92%, and 2.01%, respectively. In experiments conducted with the initial version of the proposed camera system, the error rates were calculated as 5.0%, 7.32%, 9.7%, and 7.12%, respectively. Finally, the average relative error rates for the relevant body regions of the model that performed 3D human modeling, included for comparative purposes in the experiment, were measured as 3.33%, 7.8%, 10.69%, and 12.43%, respectively.

6.1 Discussion

Analyzing the human body through anthropometric measurements presents various challenges stemming from hardware and software limitations and the human body's complexities. Several parameters, such as the subject's breathing cycle, posture, measurement timing, location, and the person conducting the measurements, can affect the results. For instance, the bust circumference varies during inhalation and exhalation, and the waist circumference differs before and after a meal or bathroom visit. Thus, it is essential to acknowledge that manual measurements may only sometimes be highly accurate. Consequently, the error rates presented in Section 5 should be interpreted cautiously.

Another notable observation from this project is the significant influence of the subject's clothing on the final model and estimated measurements. If the subject is wearing loose clothes, the body segmentation needs to be improved to fit the model accurately, leading to overestimated measurements. Additionally, the color of the clothing affects the performance of the body segmentation model. Darker colors do not reflect the light of the lasers. Hence, the software fails to detect laser points on the images, which results in an unsuccessful measurement.

Another potential factor contributing to unsuccessful measurements is the laser pointers; as explained in Section 3.2, the distance between the laser points directly impacts the calculations, and any issues with this value affect the overall outcome. The experiments demonstrated the difficulty of maintaining the stability of the laser points, as even a slight deviation from perfect alignment becomes magnified as the subject moves further away from the camera setup.

The experiments also revealed that environmental lighting and camera quality significantly impact the application's performance. Excessive brightness in the environment leads to a notable decrease in performance, as bright lights interfere with the reflections of the laser points.

The experiment results show that the proposed system is not imperfect, but there is room for further development. Improvements in both the hardware and the software components may help decrease the average error of the measurements.

One practical application of this project involves utilizing these measurements to determine the clothing size of the subject. Many clothing brands rely on bust, waist, and hip circumferences to determine the size of their customers. Therefore, the garment size that fits the individual best can be estimated using the calculated outcomes from the proposed system. However, it is essential to acknowledge that these measurements are not precise and are susceptible to errors. Additionally, size categories are often not sharply defined, and a slight change of a few centimeters can result in a different size category. A possible solution is to address this challenge by approaching size categorization as probability distributions and evaluating likelihood values. In further steps of this project, these issues can be resolved, and the proposed system can become a commercially available product used in e-commerce.

REFERENCES

[1] **Casadei, K. and Kiel, J.** (2022). *Anthropometric Measurement*, StatPearls Publishing, Treasure Island (FL), http://europepmc.org/books/NBK537315.

[2] **de Koning, L.**, **Merchant, A.T.**, **Pogue, J. and Anand, S.S.** (2007). Waist circumference and waist-to-hip ratio as predictors of cardiovascular events: meta-regression analysis of prospective studies, *European Heart Journal*, *28*(7), 850–856, https://doi.org/10.1093/eurheartj/ehm026.

[3] **Ashwell, M.**, **Gunn, P. and Gibson, S.** (2011). Waist-to-height ratio is a better screening tool than waist circumference and BMI for adult cardiometabolic risk factors: Systematic review and meta-analysis, *Obesity reviews : an official journal of the International Association for the Study of Obesity*, *13*, 275–86.

[4] **Ke, J.F.**, **Wang, J.W.**, **Lu, J.X.**, **Zhang, Z.H.**, **Liu, Y. and Li, L.X.** (2022). Waist-to-height ratio has a stronger association with cardiovascular risks than waist circumference, waist-hip ratio and body mass index in type 2 diabetes, *Diabetes Research and Clinical Practice*, *183*, 109151, https://doi.org/10.1016/j.diabres.2021.109151.

[5] **Fryar, C.**, **Gu, Q.**, **Ogden, C. and Flegal, K.** (2016). Anthropometric Reference Data for Children and Adults: United States, 2011-2014, *Vital and health statistics. Series 3, Analytical studies*, 1—46, http://europepmc.org/abstract/MED/28437242.

[6] **Zhu, S.**, **Wang, Z.**, **Heshka, S.**, **Heo, M.**, **Faith, M.S. and Heymsfield, S.B.** (2002). Waist circumference and obesity-associated risk factors among whites in the third National Health and Nutrition Examination Survey: clinical action thresholds, *The American Journal of Clinical Nutrition*, *76*(4), 743–743, https://doi.org/10.1093/ajcn/76.4.743.

[7] **Borel, A.L.**, **Coumes, S.**, **Reche, F.**, **Ruckly, S.**, **Pépin, J.L.**, **Tamisier, R.**, **Wion, N. and Arvieux, C.** (2018). Waist, neck circumferences, waist-to-hip ratio: Which is the best cardiometabolic risk marker in women with severe obesity? The SOON cohort, *PLOS ONE*, *13*(11), e0206617, https://doi.org/10.1371/journal.pone.0206617.

[8] **Casadei, K. and Kiel, J.** (2021). Anthropometric measurement, *StatPearls [Internet]*.

[9] **Janssen, I., Katzmarzyk, P.T. and Ross, R.** (2004). Waist circumference and not body mass index explains obesity-related health risk, *The American Journal of Clinical Nutrition*, *79*(3), 379–384, https://doi.org/10.1093/ajcn/79.3.379.

[10] **Maffeis, C., Pietrobelli, A., Grezzani, A., Provera, S. and Tatò, L.** (2001). Waist Circumference and Cardiovascular Risk Factors in Prepubertal Children, *Obesity Research*, *9*(3), 179–187, https://doi.org/10.1038/oby.2001.19.

[11] **Janghorbani, M., Momeni, F. and Dehghani, M.** (2012). Hip circumference, height and risk of type 2 diabetes: systematic review and meta-analysis, *Obesity Reviews*, *13*(12), 1172–1181, https://doi.org/10.1111/j.1467-789x.2012.01030.x.

[12] **Cameron, A.J., Magliano, D.J. and Söderberg, S.** (2012). A systematic review of the impact of including both waist and hip circumference in risk models for cardiovascular diseases, diabetes and mortality, *Obesity Reviews*, *14*(1), 86–94, https://doi.org/10.1111/j.1467-789x.2012.01051.x.

[13] **Rumbo-Rodríguez, L., Sánchez-SanSegundo, M., Ferrer-Cascales, R., García-D'Urso, N., Hurtado-Sánchez, J.A. and Zaragoza-Martí, A.** (2021). Comparison of Body Scanner and Manual Anthropometric Measurements of Body Shape: A Systematic Review, *International Journal of Environmental Research and Public Health*, *18*(12), 6213, https://doi.org/10.3390/ijerph18126213.

[14] **Kaashki, N.N., Hu, P. and Munteanu, A.** (2021). Anet: A Deep Neural Network for Automatic 3D Anthropometric Measurement Extraction, *IEEE Transactions on Multimedia*, 1–1, https://doi.org/10.1109/tmm.2021.3132487.

[15] **Bretschneider, T., Koop, U., Schreiner, V., Wenck, H. and Jaspers, S.** (2009). Validation of the body scanner as a measuring tool for a rapid quantification of body shape, *Skin Research and Technology*, *15*(3), 364–369, https://doi.org/10.1111/j.1600-0846.2009.00374.x.

[16] **Ng, B.K., Hinton, B.J., Fan, B., Kanaya, A.M. and Shepherd, J.A.** (2016). Clinical anthropometrics and body composition from 3D whole-body surface scans, *European Journal of Clinical Nutrition*, *70*(11), 1265–1270, https://doi.org/10.1038/ejcn.2016.109.

[17] **Weiss, E.T., Barzilai, O., Brightman, L., Chapas, A., Hale, E., Karen, J., Bernstein, L. and Geronemus, R.G.** (2009). Three-dimensional surface imaging for clinical trials: Improved precision and reproducibility in circumference measurements of thighs and abdomens, *Lasers in Surgery and Medicine*, *41*(10), 767–773, https://doi.org/10.1002/lsm.20863.

[18] **Sheth, M. and Srivastava, N.** (2020). *Predicting Body Size Using Mirror Selfies*, volume11886 LNCS of *Lecture Notes in Computer Science (including subseries Lecture Notes in Artificial Intelligence and Lecture Notes in Bioinformatics)*, Springer, www.scopus.com.

[19] **Hung, P.**, **Witana, C. and Goonetilleke, R.** (2004). Anthropometric Measurements from Photographic Images, *Computing Systems*, *29*.

[20] **Meunier, P. and Yin, S.** (2000). Performance of a 2D image-based anthropometric measurement and clothing sizing system, *Applied Ergonomics*, *31*(5), 445–451, https://doi.org/10.1016/s0003-6870(00)00023-5.

[21] **Utkualp, N. and Ercan, I.** (2015). Anthropometric Measurements Usage in Medical Sciences, *BioMed Research International*, *2015*, 1–7, https://doi.org/10.1155/2015/404261.

[22] **Siren, R.**, **Eriksson, J.G. and Vanhanen, H.** (2012). Waist circumference a good indicator of future risk for type 2 diabetes and cardiovascular disease, *BMC public health*, *12*(1), 1–6.

[23] **Vasiljevic, I.**, **Gardasevic, J.**, **Kezunovic, M. and Bojanic, D.** (2017). Waist circumference as an indicator abdominal obesity in middle age, *Sport Mont*, *15*(1), 21–22.

[24] **Chen, B. and Li, H.f.** (2011). Waist circumference as an indicator of high blood pressure in preschool obese children, *Asia Pacific Journal of Clinical Nutrition*, *20*(4), 557–562, https://search.informit.org/doi/10.3316/ielapa.688483583414376.

[25] **Łopatyński, J.**, **Mardarowicz, G. and Szcześniak, G.** (2003). A comparative evaluation of waist circumference, waist-to-hip ratio, waist-to-height ratio and body mass index as indicators of impaired glucose tolerance and as risk factors for type-2 diabetes mellitus, *Annales Universitatis Mariae Curie-Sklodowska. Sectio D: Medicina*, *58*(1), 413—419, http://europepmc.org/abstract/MED/15315025.

[26] **Rezende, F.A.C.**, **Rosado, L.E.F.P.L.**, **de Cássia Lanes Ribeiro, R.**, **de Carvalho Vidigal, F.**, **Vasques, A.C.J.**, **Bonard, I.S. and de Carvalho, C.R.** (2006). Índice de massa corporal e circunferência abdominal: associação com fatores de risco cardiovascular, *Arquivos Brasileiros de Cardiologia*, *87*(6), https://doi.org/10.1590/s0066-782x2006001900008.

[27] **Parker, E.D.**, **Pereira, M.A.**, **Stevens, J. and Folsom, A.R.** (2009). Association of hip circumference with incident diabetes and coronary heart disease: the Atherosclerosis Risk in Communities study, *American journal of epidemiology*, *169*(7), 837–847.

[28] **Cameron, A.J.**, **Magliano, D.J.**, **Shaw, J.E.**, **Zimmet, P.Z.**, **Carstensen, B.**, **Alberti, K.G.M.**, **Tuomilehto, J.**, **Barr, E.L.**, **Pauvaday, V.K.**, **Kowlessur, S.** *et al.* (2012). The influence of hip circumference on the relationship between abdominal obesity and mortality, *International journal of epidemiology*, *41*(2), 484–494.

[29] **Heitmann, B. and Lissner, L.** (2011). Hip Hip Hurrah! Hip size inversely related to heart disease and total mortality, *Obesity Reviews*, *12*(6), 478–481.

[30] **Sayeed, M.**, **Mahtab, H.**, **Latif, Z.**, **Khanam, P.**, **Ahsan, K.**, **Banu, A. and Azad Khan, A.** (2003). Waist-to-height ratio is a better obesity index than body mass index and waist-to-hip ratio for predicting diabetes, hypertension and lipidemia, *Bangladesh Medical Research Council bulletin*, *29*(1), 1—10, `http://europepmc.org/abstract/MED/14674615`.

[31] **Xu, Z.**, **Qi, X.**, **Dahl, A.K. and Xu, W.** (2013). Waist-to-height ratio is the best indicator for undiagnosed Type 2 diabetes, *Diabetic Medicine*, *30*(6), e201–e207, `https://doi.org/10.1111/dme.12168`.

[32] **Gibson, S. and Ashwell, M.** (2020). A simple cut-off for waist-to-height ratio (0·5) can act as an indicator for cardiometabolic risk: recent data from adults in the Health Survey for England, *British Journal of Nutrition*, *123*(6), 681–690.

[33] **Shen, S.**, **Lu, Y.**, **Qi, H.**, **Li, F.**, **Shen, Z.**, **Wu, L.**, **Yang, C.**, **Wang, L.**, **Shui, K.**, **Yao, W.** *et al.* (2017). Waist-to-height ratio is an effective indicator for comprehensive cardiovascular health, *Scientific reports*, *7*(1), 1–7.

[34] **Balat, K.**, , **Pazarli, A.C.**, **Koseoglu, H.I.**, **Yasayancan, N.**, **Demir, O.**, , **and and** (2021). Importance of Anthropometric Measurements to Determine Cardiometabolic Diseases in Obstructive Sleep Apnea Syndrome, *Turkish Thoracic Journal*, *22*(1), 11–17, `https://doi.org/10.5152/turkthoracj.2020.19105`.

[35] **Seidell, J.C.** (2009). Waist circumference and waist/hip ratio in relation to all-cause mortality, cancer and sleep apnea, *European Journal of Clinical Nutrition*, *64*(1), 35–41, `https://doi.org/10.1038/ejcn.2009.71`.

[36] **Akpinar, E.**, **Bashan, I.**, **Bozdemir, N. and Saatci, E.** (2007). Which is the best anthropometric technique to identify obesity: body mass index, waist circumference or waist-hip ratio?, *Collegium antropologicum*, *31*(2), 387–393.

[37] **Esmaillzadeh, A.**, **Mirmiran, P. and Azizi, F.** (2004). Waist-to-hip ratio is a better screening measure for cardiovascular risk factors than other anthropometric indicators in Tehranian adult men, *International Journal of Obesity*, *28*(10), 1325–1332, `https://doi.org/10.1038/sj.ijo.0802757`.

[38] **Xiao, Y., Liu, Y., Zheng, S., Yang, Y., Fan, S., Yang, C., Zhang, J. and Ye, Y.** (2016). [Relationship between hypertension and body mass index, waist circumference and waist-hip ratio in middle-aged and elderly residents], *Zhonghua liu xing bing xue za zhi = Zhonghua liuxingbingxue zazhi*, *37*(9), 1223—1227, `https://doi.org/10.3760/cma.j.issn.0254-6450.2016.09.008`.

[39] **Meunier, P. and Yin, S.** (2000). Performance of a 2D image-based anthropometric measurement and clothing sizing system, *Applied Ergonomics*, *31*(5), 445–451, `https://www.sciencedirect.com/science/article/pii/S0003687000000235`.

[40] **Farina, G., Spataro, F., Lorenzo, A.D. and Lukaski, H.** (2016). A Smartphone Application for Personal Assessments of Body Composition and Phenotyping, *Sensors*, *16*(12), 2163, `https://doi.org/10.3390/s16122163`.

[41] **Pradhan, L., Song, G., Zhang, C., Gower, B., Heymsfield, S.B., Allison, D.B. and Affuso, O.** (2015). Feature Extraction from 2D Images for Body Composition Analysis, *2015 IEEE International Symposium on Multimedia (ISM)*, pp.45–52.

[42] **Shah, J., Shah, C., Sandhu, H., Shaikh, M. and Natu, P.** (2019). A Methodology For Extracting Anthropometric Measurements from 2D Images, *2019 International Conference on Advances in Computing, Communication and Control (ICAC3)*, IEEE, pp.1–6, `https://doi.org/10.1109/icac347590.2019.9036788`.

[43] **de Souza, J.W.M., Holanda, G.B., Ivo, R.F., Alves, S.S.A., da Silva, S.P.P., Nunes, V.X., Loureiro, L.L., Dias-Silva, C.H. and Rebouças Filho, P.P.** (2020). Predicting body measures from 2D images using Convolutional Neural Networks, *2020 International Joint Conference on Neural Networks (IJCNN)*, pp.1–6.

[44] **Paquette, S., Brantley, J.D., Corner, B.D., Li, P. and Oliver, T.** (2000). Automated extraction of anthropometric data from 3D images, *Proceedings of the Human Factors and Ergonomics Society Annual Meeting*, volume 44, SAGE Publications Sage CA: Los Angeles, CA, pp.727–730.

[45] **Kaashki, N.N., Hu, P. and Munteanu, A.** (2023). Anet: A Deep Neural Network for Automatic 3D Anthropometric Measurement Extraction, *IEEE Transactions on Multimedia*, *25*, 831–844.

[46] **Kaashki, N.N., Hu, P. and Munteanu, A.** (2021). Deep Learning-Based Automated Extraction of Anthropometric Measurements From a Single 3-D Scan, *IEEE Transactions on Instrumentation and Measurement*, *70*, 1–14.

[47] **Łukasz Markiewicz, Witkowski, M., Sitnik, R. and Mielicka, E.** (2017). 3D anthropometric algorithms for the estimation of measurements required

for specialized garment design, *Expert Systems with Applications*, *85*, 366–385, https://www.sciencedirect.com/science/article/pii/S0957417417303007.

[48] **Jamil, A.**, **Herodian, S. and Saulia, L.** (2020). RGB-D sensor application for static anthropometry measurement, *IOP Conference Series: Earth and Environmental Science*, *542*(1), 012036, https://doi.org/10.1088/1755-1315/542/1/012036.

[49] **Shah, C.**, **Shah, J.**, **Shaikh, M.**, **Sandhu, H. and Natu, P.** (2022). Anthropometric Measurement Technology Using 2D Images, ***S. Shakya**, **K.L. Du and W. Haoxiang**, editors, Proceedings of Second International Conference on Sustainable Expert Systems*, Springer Nature Singapore, Singapore, pp.127–142.

[50] **Abadi, M.**, **Agarwal, A.**, **Barham, P.**, **Brevdo, E.**, **Chen, Z.**, **Citro, C.**, **Corrado, G.S.**, **Davis, A.**, **Dean, J.**, **Devin, M.**, **Ghemawat, S.**, **Goodfellow, I.**, **Harp, A.**, **Irving, G.**, **Isard, M.**, **Jia, Y.**, **Jozefowicz, R.**, **Kaiser, L.**, **Kudlur, M.**, **Levenberg, J.**, **Mané, D.**, **Monga, R.**, **Moore, S.**, **Murray, D.**, **Olah, C.**, **Schuster, M.**, **Shlens, J.**, **Steiner, B.**, **Sutskever, I.**, **Talwar, K.**, **Tucker, P.**, **Vanhoucke, V.**, **Vasudevan, V.**, **Viégas, F.**, **Vinyals, O.**, **Warden, P.**, **Wattenberg, M.**, **Wicke, M.**, **Yu, Y. and Zheng, X.** (2015). *TensorFlow: Large-Scale Machine Learning on Heterogeneous Systems*, https://www.tensorflow.org/, software available from tensorflow.org.

[51] **Lugaresi, C.**, **Tang, J.**, **Nash, H.**, **McClanahan, C.**, **Uboweja, E.**, **Hays, M.**, **Zhang, F.**, **Chang, C.L.**, **Yong, M.G.**, **Lee, J.**, **Chang, W.T.**, **Hua, W.**, **Georg, M. and Grundmann, M.** (2019). *MediaPipe: A Framework for Building Perception Pipelines*, https://arxiv.org/abs/1906.08172.

[52] **URL-1** (2023). https://developers.google.com/mediapipe/solutions/guide, [Online; accessed 15-June-2023].

[53] **URL-2** (2023). https://developers.google.com/mediapipe/solutions/vision/pose_landmarker, [Online; accessed 15-June-2023].

[54] **Howard, A.G.**, **Zhu, M.**, **Chen, B.**, **Kalenichenko, D.**, **Wang, W.**, **Weyand, T.**, **Andreetto, M. and Adam, H.** (2017). *MobileNets: Efficient Convolutional Neural Networks for Mobile Vision Applications*, https://arxiv.org/abs/1704.04861.

[55] **He, K.**, **Zhang, X.**, **Ren, S. and Sun, J.** (2015). *Deep Residual Learning for Image Recognition*, 1512.03385.

[56] **URL-3** (2023). https://blog.tensorflow.org/2019/11/updated-bodypix-2.html, [Online; accessed 15-June-2023].

[57] **Oved, D.**, **Zhu, T. and Alvarado, I.** (2021). *BodyPix: Real-time Person Segmentation in the Browser with TensorFlow. js. 2019*.

[58] **Loper, M.**, **Mahmood, N.**, **Romero, J.**, **Pons-Moll, G. and Black, M.J.** (2015). SMPL: A Skinned Multi-Person Linear Model, *ACM Trans. Graphics (Proc. SIGGRAPH Asia)*, *34*(6), 248:1–248:16.

[59] **Li, Z.**, **Yu, X.**, **Lian, X.**, **Wang, Y. and Ji, X.** (2022). *Human Health Indicator Prediction from Gait Video*, `2212.12948`.

[60] **Thankur, R.P.**, **Pujades, S.**, **Goel, L.**, **Pohmann, R.**, **Machann, J. and Black, M.J.** (2020). GENTEL : GENerating Training data Efficiently for Learning to segment medical images, *RFIAP 2020 - Congrés Reconnaissance des Formes, Image, Apprentissage et Perception*, Vannes, France, pp.1–7, `https://inria.hal.science/hal-02988367`.

[61] **Guo, H.**, **Planche, B.**, **Zheng, M.**, **Karanam, S.**, **Chen, T. and Wu, Z.** (2022). SMPL-A: Modeling Person-Specific Deformable Anatomy, *Proceedings of the IEEE/CVF Conference on Computer Vision and Pattern Recognition (CVPR)*, pp.20814–20823.

[62] **Chung, Y.Y.**, **Guo, H.J.**, **Kumar, H.G. and Prabhakaran, B.** (2020). High-quality First-person Rendering Mixed Reality Gaming System for In Home Setting, *2020 IEEE International Conference on Artificial Intelligence and Virtual Reality (AIVR)*, pp.339–344.

[63] **Bebko, A.O.**, **Thaler, A. and Troje, N.F.** (2021). bmlSUP – A SMPL Unity Player, *2021 IEEE Conference on Virtual Reality and 3D User Interfaces Abstracts and Workshops (VRW)*, pp.573–574.

[64] **Cai, Z.**, **Zhang, M.**, **Ren, J.**, **Wei, C.**, **Ren, D.**, **Lin, Z.**, **Zhao, H.**, **Yang, L.**, **Loy, C.C. and Liu, Z.** (2022). *Playing for 3D Human Recovery*, `2110.07588`.

[65] **URL-4** (2023). `https://meshcapade.com/about-us`, [Online; accessed 15-June-2023].

[66] **URL-5** (2023). `https://meshcapade.com`, [Online; accessed 15-June-2023].

[67] **Bradski, G.** (2000). The OpenCV Library, *Dr. Dobb's Journal of Software Tools*.

[68] **Hunter, J.D.** (2007). Matplotlib: A 2D graphics environment, *Computing in Science & Engineering*, *9*(3), 90–95.

[69] **Wes McKinney** (2010). Data Structures for Statistical Computing in Python, ***Stéfan van der Walt and Jarrod Millman****, editors, Proceedings of the 9th Python in Science Conference*, pp.56 – 61.

[70] **Harris, C.R.**, **Millman, K.J.**, **van der Walt, S.J.**, **Gommers, R.**, **Virtanen, P.**, **Cournapeau, D.**, **Wieser, E.**, **Taylor, J.**, **Berg, S.**, **Smith, N.J.**, **Kern, R.**, **Picus, M.**, **Hoyer, S.**, **van Kerkwijk, M.H.**, **Brett, M.**, **Haldane, A.**, **del Río, J.F.**, **Wiebe, M.**, **Peterson, P.**, **Gérard-Marchant, P.**, **Sheppard, K.**, **Reddy, T.**, **Weckesser, W.**, **Abbasi, H.**, **Gohlke, C. and Oliphant, T.E.** (2020). Array programming with NumPy, *Nature*, *585*(7825), 357–362, `https://doi.org/10.1038/s41586-020-2649-2`.

[71] **Grinberg, M.** (2018). *Flask web development: developing web applications with python*, " O'Reilly Media, Inc.".

[72] **Smith, S.C. and Haslam, D.** (2006). Abdominal obesity, waist circumference and cardiometabolic risk: awareness among primary care physicians, the general population and patients at risk – the Shape of the Nations survey, *Current Medical Research and Opinion*, *23*(1), 29–47, `https://doi.org/10.1185/030079906x159489`.

[73] **Hu, F.B.** (2007). Obesity and Mortality, *Archives of Internal Medicine*, *167*(9), 875, `https://doi.org/10.1001/archinte.167.9.875`.

[74] **Ross, R.**, **Berentzen, T.**, **Bradshaw, A.J.**, **Janssen, I.**, **Kahn, H.S.**, **Katzmarzyk, P.T.**, **Kuk, J.L.**, **Seidell, J.C.**, **Snijder, M.B.**, **Sørensen, T.I.A. and Després, J.P.** (2008). Does the relationship between waist circumference, morbidity and mortality depend on measurement protocol for waist circumference?, *Obesity Reviews*, *9*(4), 312–325, `https://doi.org/10.1111/j.1467-789x.2007.00411.x`.

[75] **Ferrucci, M.**, **Doiron, T.D.**, **Thompson, R.M.**, **Jones, J.P.**, **Freeman, A.J. and Neiman, J.A.** (2016). Dimensional review of scales for forensic photography, *Journal of forensic sciences*, *61*(2), 509–519.

APPENDICES

APPENDIX A : Tables for Bust Circumferences
APPENDIX B : Tables for Waist Circumferences
APPENDIX C : Tables for Hip Circumferences
APPENDIX D : Tables for Height

APPENDIX A : Tables for Bust Circumferences

This section presents the tables that contain the relative errors between the estimations of the proposed model and the real bust circumferences for each human subject who participated in the experiments.

Table A.1 : Bust circumferences calculated from images captured with camera version 1.

Subject No	Manual (cm)	Automatic (cm)	Error (%)	Average Error (%)
2	88	109.16	24.04	23.93
		108.97	23.82	
3	90	93.48	3.86	2.7
		88.62	1.53	
4	105	99.11	5.6	2.86
		105.13	0.12	
9	97	106.85	10.15	6.95
		100.65	3.76	
10	95	98.61	3.8	2.02
		94.76	0.25	
11	98	95.08	2.97	5.45
		105.78	7.93	
12	96	106.87	11.32	11.32
13	97	95.62	1.42	2.01
		99.53	2.6	
15	92	97.89	6.4	8.97
		102.63	11.55	
16	92	91.57	0.46	6.48
		103.51	12.51	
17	77	90.8	17.92	9.5
		77.84	1.09	
18	86	82.33	4.26	3.25
		84.07	2.24	
19	80	85.75	7.18	9.75
		89.86	12.32	

Table A.2 : Bust circumferences calculated from images captured with camera version 2.

Subject No	Manual (cm)	Automatic (cm)	Error (%)	Average Error (%)
1	101	116.62 112.64	15.46 11.52	13.49
2	88	116.13 116.11	31.96 31.94	31.95
3	90	96.14 99.09	6.82 10.1	8.46
5	89	107.08 107.47	20.31 20.75	20.53
9	97	121.09 123.33	24.83 27.14	25.98
10	95	98.97 98.84	4.17 4.04	4.11
11	98	94.31 113.34	3.76 15.65	9.7
12	96	110.92 116.02	15.54 20.85	18.19
13	97	107.97 99.3	11.3 2.37	6.84
14	94	103	9.57	9.57
15	92	117.97 117.29	28.22 27.48	27.85
16	92	91.57 103.51	0.46 12.51	6.48
19	80	88.06 95.85	10.07 19.81	14.94

Table A.3 : Bust circumferences calculated with SMPL model

Subject No	Manual (cm)	Automatic (cm)	Error (%)	Average Error (%)
1	101	117.09 110.07	15.93 8.98	12.45
2	88	92.31 87.95	4.89 0.05	2.47
3	90	106.79 105.04	18.65 16.71	17.68
4	105	101.17 98.06	3.64 6.6	5.12
5	89	93.29 96.28	4.82 8.17	6.5
9	97	91.38 91.18	5.79 6	5.89
10	95	95.5 95.01	0.52 0.01	0.26
11	98	94.01 92.34	4.07 5.77	4.92
12	96	105.76 106.67	10.16 11.11	10.64
13	97	93.96 90.47	3.13 6.73	4.93
14	94	104.22 101.68	10.87 8.17	9.52
15	92	94.7 93.6	2.93 1.73	2.33
16	92	80.49 76.62	12.51 16.71	14.61
17	77	93.65 101.25	21.62 31.49	26.55
18	86	84.94 72.16	1.23 16.09	8.66
19	80	73.98 76.93	7.525 3.86	5.68

APPENDIX B : Tables for Waist Circumferences

This section presents the tables that contain the relative errors between the estimations of the proposed model and the real waist circumferences for each human subject who participated in the experiments.

Table B.1 : Waist circumferences calculated from images captured with camera version 1.

Subject No	Manual (cm)	Automatic (cm)	Error (%)	Average Error (%)
2	79	81.39	3.02	5.33
		85.04	7.64	
3	75	85.5	14.0	12.13
		82.7	10.26	
4	100	91.6	8.4	6.84
		94.71	5.29	
9	87	94.48	8.59	4.45
		86.73	0.31	
10	82	85.27	3.98	2.69
		86.73	1.40	
11	84	97.58	16.16	16.00
		97.31	15.84	
12	97	95.65	1.39	1.39
13	97	85.76	11.58	9.15
		90.48	6.72	
15	79	85.97	8.82	8.13
		84.88	7.44	
16	75	80.33	7.10	15.38
		92.75	23.6	
17	66	90.18	36.63	34.71
		87.64	32.78	
18	69	68.8	0.28	0.75
		69.84	1.21	
19	71	75.58	6.45	9.22
		79.52	12	

Table B.2 : Waist circumferences calculated from images captured with camera version 2.

Subject No	Manual (cm)	Automatic (cm)	Error (%)	Average Error (%)
1	100	101.47 101.25	1.47 1.25	1.36
2	79	88.32 87.31	11.79 10.51	11.15
3	75	89.71 91.91	19.61 22.54	21.08
5	89	95.84 93.93	7.68 5.53	6.61
9	87	100.7 103.59	15.74 19.06	17.4
10	82	88.15 88.94	7.5 8.46	7.98
11	84	84.65 101.21	0.77 20.48	10.63
12	97	101.94 104.4	5.06 7.62	6.34
13	97	95.07 94.39	1.98 2.69	2.34
14	89	90.56	1.75	1.75
15	79	101.19 100.91	28.08 27.73	27.91
19	71	74.17 74.26	4.46 4.59	4.52

Table B.3 : Waist circumferences calculated with SMPL model

Subject No	Manual (cm)	Automatic (cm)	Error (%)	Average Error (%)
1	100	104.99 97.36	4.99 2.64	3.81
2	79	75.94 70.08	3.87 11.29	7.58
3	75	86.02 82.29	14.69 9.72	12.2
4	100	88.48 90.15	11.52 8.85	10.68
5	89	79.43 83.04	10.75 6.69	8.72
9	87	74.09 72.06	14.83 17.17	16.0
10	82	87.87 86.53	7.15 5.52	6.34
11	84	73.61 74.88	12.36 10.85	11.61
12	97	97.04 95.78	0.04 1.25	0.64
13	97	77.21 75.9	20.4 21.75	21.07
14	89	90.0 89.89	1.12 1.0	1.06
15	79	75.12 72.34	4.91 8.43	6.67
16	75	63.32 63.02	15.57 15.97	15.77
17	66	88.91 91.54	34.71 38.69	36.7
18	69	59.85 65.4	13.26 5.21	9.23
19	71	60.47 67.37	14.83 5.11	9.97

APPENDIX C : Tables for Hip Circumferences

This section presents the tables that contain the relative errors between the estimations of the proposed model and the real hip circumferences for each human subject who participated in the experiments.

Table C.1 : Hip circumferences calculated from images taken with camera version 1.

Subject No	Manual (cm)	Automatic (cm)	Error (%)	Average Error (%)
2	98	90.44	7.71	5.85
		94.09	3.98	
3	101	94.16	6.77	8.14
		91.38	9.52	
4	104	95.12	8.53	6.88
		98.55	5.24	
9	101	94.28	6.65	8.82
		89.9	10.99	
10	98	98.07	0.07	0.03
		82.33	15.98	
11	106	107.77	1.66	1.46
		107.33	1.25	
12	109	108.5	0.45	0.45
13	103	94.87	7.89	6.61
		97.51	5.33	
15	100	91.62	8.38	7.85
		92.67	7.33	
16	96	92.18	3.97	2.65
		94.73	1.32	
17	92	89.26	2.97	2.4
		90.32	1.82	
18	98	80.0	18.36	20.07
		76.66	21.77	
19	102	88.54	13.19	13.4
		88.12	13.6	

Table C.2 : Hip circumferences calculated from images taken with camera version 2.

Subject No	Manual (cm)	Automatic (cm)	Error (%)	Average Error (%)
1	111	108.89	1.9	1.42
		109.94	0.95	
2	98	100.05	2.09	2.09
		100.05	2.09	
3	101	100.17	0.82	1.03
		99.74	1.24	
5	108	112.28	3.96	3.96
		112.28	3.96	
9	101	102.18	1.16	1.16
		102.17	1.15	
10	98	97.28	0.73	0.92
		99.1	1.12	
11	106	105.16	0.79	0.73
		106.72	0.67	
12	109	112.61	3.31	4.03
		114.18	4.75	
13	103	104.26	1.22	1.65
		105.14	2.07	
14	100	94.32	5.68	5.68
15	100	100.36	0.36	0.46
		100.56	0.56	
19	102	101.38	0.6	1.06
		100.45	1.51	

Table C.3 : Hip circumferences calculated with SMPL model

Subject No	Manual (cm)	Automatic (cm)	Error (%)	Average Error (%)
1	111	109.6 104.13	1.26 6.18	3.72
2	98	87.68 82.74	10.53 15.57	13.05
3	101	94.4 90.79	6.53 10.1	8.32
4	104	89.09 91.54	14.33 11.98	13.15
5	108	90.02 91.96	16.64 14.85	15.75
6	106	89.26 86.14	15.79 18.73	17.26
7	116	92.66 92.15	20.12 20.56	20.34
8	90	83.11 83.6	7.65 7.11	7.38
9	101	81.23 80.39	19.57 20.4	19.99
10	98	95.26 93.64	2.79 4.44	3.62
11	106	80.96 86.03	23.62 18.83	21.23
12	109	105.25 103.89	3.44 4.68	4.06
13	103	84.71 83.78	17.75 18.66	18.2
14	100	98.5 96.6	1.5 3.4	2.45
15	100	87.8 87.41	12.2 12.59	12.39
16	96	82.0 79.88	14.58 16.79	15.68
17	92	81.48 96.1	11.43 4.45	7.94
18	98	79.28 82.56	19.1 15.75	17.42
19	102	86.43 88.48	15.26 13.25	14.25

APPENDIX D : Tables for Height

This section presents the tables that contain the relative errors between the estimations of the proposed model and the real height for each human subject who participated in the experiments.

Table D.1 : Height calculated from images captured with camera version 1.

Subject No	Manual (cm)	Automatic (cm)	Error (%)	Average Error (%)
2	175	164.79 170.5	5.83 2.57	4.2
4	172	165.22 165.68	3.94 3.67	3.8
9	182	179.46 188.01	1.39 3.3	2.34
10	175	154.2 155.48	11.88 11.15	11.52
11	183	188.76 174.98	3.14 4.38	3.76
13	173	168.73 176.0	2.46 1.73	2.1
15	173	163.94 163.73	5.23 5.35	5.29
16	183	170.32 158.96	6.92 13.13	10.03
17	167	168.8	1.07	1.07
18	173	161.4	6.7	6.7
19	170	162.52 163.35	4.4 3.91	4.15

Table D.2 : Height calculated from images captured with camera version 2.

Subject No	Manual (cm)	Automatic (cm)	Error (%)	Average Error (%)
1	178	182.14	2.32	2.59
		183.09	2.85	
2	175	177.59	1.48	1.53
		177.77	1.58	
5	170	170.0	0	0.06
		169.77	0.13	
9	182	190.43	4.63	5.76
		194.56	6.9	
10	175	183.26	4.72	3.41
		178.69	2.1	
11	183	196.66	7.46	7.33
		196.19	7.2	
12	183	177.69	2.9	2.87
		188.2	2.84	
13	173	177.17	2.41	2.37
		177.04	2.33	
14	180	161.44	10.31	10.31
15	173	189.28	9.41	9.41
		189.28	9.41	
19	170	175.89	3.46	3.07
		174.56	2.68	

Table D.3 : Height calculated with SMPL model

Subject No	Manual (cm)	Automatic (cm)	Error (%)	Average Error (%)
1	178	179.01	0.56	1.58
		173.36	2.6	
2	175	181.95	3.97	2.52
		176.88	1.07	
3	160	182.03	13.76	11.17
		173.74	8.58	
4	172	177.13	2.98	2.67
		176.07	2.36	
5	170	175.32	3.12	3.67
		177.16	4.21	
6	180	176.11	2.16	1.77
		177.51	1.38	
7	185	175.99	4.87	4.64
		176.83	4.41	
8	174	180.36	3.65	2.96
		177.97	2.28	
9	182	181.8	0.1	0.19
		181.5	0.27	
10	175	176.84	1.05	1.82
		179.53	2.58	
11	183	183.29	0.15	0.78
		180.43	1.4	
12	183	176.86	3.35	3.08
		177.85	2.81	
13	173	177.05	2.34	2.63
		178.08	2.93	
14	180	173.1	3.83	3.08
		175.79	2.33	
15	173	181.8	5.08	4.96
		181.37	4.83	
16	183	182.41	0.32	0.92
		180.21	1.52	
17	167	181.32	8.57	7.98
		179.35	7.39	
18	173	177.77	2.75	3.5
		180.35	4.24	
19	170	177.05	4.14	3.36
		174.4	2.58	

CURRICULUM VITAE

Rumeysa Aslıhan ERTÜRK

EDUCATION:

- **B.Sc.:** 2020, Istanbul Technical University, Faculty of Computer and Informatics, Computer Engineering Department

PROFESSIONAL EXPERIENCE AND REWARDS:

- 2020-2021, Istanbul University, Data Scientist at the Department of Astronomy and Space Sciences.
- 2021- , Istanbul Technical University, Research Assistant at Department of Computer Engineering.

PUBLICATIONS, PRESENTATIONS AND PATENTS ON THE THESIS:

- **Ertürk R. A.**, Kamaşak M.E., (2022). Anthropometric Measurements with 2D Images *2022 7th International Conference on Computer Science and Engineering (UBMK)*, September, 2007 Diyarbakır, Türkiye. (Presentation Instance)